GAS MIXING IN CONICAL SPOUTED BEDS

A THESIS SUBMITTED TO
THE GRADUATE SCHOOL OF NATURAL AND APPLIED SCIENCES
OF
MIDDLE EAST TECHNICAL UNIVERSITY

BY

NESLİN DOĞAN

IN PARTIAL FULFILLMENT OF THE REQUIREMENTS
FOR
THE DEGREE OF MASTER OF SCIENCE
IN
CHEMICAL ENGINEERING

DECEMBER 2020

Approval of the Thesis:

I hereby declare that all information in this document has been obtained and presented in accordance with academic rules and ethical conduct. I also declare that, as required by these rules and conduct, I have fully cited and referenced all material and results that are not original to this work.

Name, Surname:

Signature:

ABSTRACT

GAS MIXING IN CONICAL SPOTED BEDS

Doğan, Neslin
Master of Science, Chemical Engineering
Supervisor : Prof. Dr. Görkem Külah

December 2020, 86 pages

Conical spouted beds are relatively new generation gas-solid flow reactors used in various applications such as drying, catalytic polymerization, treatment of wastes, particle coating and chemical vapor deposition due to their advantages over cylindrical spouted beds. For complete characterization of conical spouted beds, determination of the local flow structure based on gas velocity and gas mixing is of paramount importance. There are limited studies on local gas behavior in conical spouted beds, especially operating with high-density particles. Therefore, the objective of this thesis study was to investigate the effect of particle density, bed size and conical angle on the local gas behavior and the axial gas mixing behavior in conical spouted beds.

Local gas velocity measurements were conducted utilizing a Pitot tube in two small scale (D_c = 150 mm, γ = 30º, 60º) and one large scale (D_c = 250 mm, γ = 66º) conical spouted beds. Three different types of particles; zirconia (ρ_p = 6050 kg/m^3), zirconia toughened alumina (ρ_p = 3700 kg/m^3) and glass beads (ρ_p = 2460 kg/m^3), were used in the experiments. Careful calibration of the Pitot tube for determination of gas velocities in the annulus section was carried out in a separate loosely packed bed set-up, which represents the flow conditions in the annulus section of the spouted bed. Effects of axial position, conical angle, bed size and particle density on gas velocity profiles were investigated. It is shown that the amount of air flows through the annulus increases as the axial distance and particle density increases; however, it decreases with increasing cone angle. Dispersion of the gas into the annulus is found to be significantly higher in the large-scale unit than the small-scale unit.

Local gas velocity measurements conducted in small scale conical spouted beds were used in a 1-D convection-diffusion gas mixing model to quantify the axial gas mixing characteristics of conical spouted beds. . The developed gas mixing model based on San Jose et al (1995) was implemented in MATLAB and dispersion coefficients for all operating conditions were determined. The results show that the dispersion coefficients obtained in this study have an order of 10^{-2} m^2/s and are higher than the corresponding dispersion coefficients of fixed beds, lower than the corresponding dispersion coefficients of fluidized beds and similar with the cylindrical spouted beds reported in the literature. In addition, Peclet numbers found in the range of 0.56-7.84 revealed that the convective transport was more dominant than axial dispersion for light particles compared to heavy particles.

Keywords: Conical Spouted Bed, High-density Particles, Local Gas Velocity, Pitot tube, Gas Dispersion Coefficient

ÖZ

KONİK TABANLI TAŞKIN YATAKLARDA GAZ KARIŞIMI

Doğan, Neslin
Yüksek Lisans, Kimya Mühendisliği
Tez Yöneticisi: Prof. Dr. Görkem Külah

Aralık 2020, 86 sayfa

Lokal gaz hızı ölçümleri, iki küçük ölçekli (D_c = 150 mm, **γ** = 30º, 60º) ve bir büyük ölçekli (D_c = 250 mm, **γ** = 66º) konik tabanlı taşkın yataklarda Pitot tüpü kullanılarak gerçekleştirilmiştir. Deneylerde zirkonya (ρ_p = 6050 kg/m^3), zirkonya ile sertleştirilmiş alümina (ρ_p = 3700 kg/m^3) ve cam boncuk (ρ_p = 2460 kg/m^3) olmak üzere üç farklı parçacık kullanılmıştır. Halka bölgesindeki hızların belirlenmesi için Pitot tüpün dikkatli kalibrasyonu, taşkın yatağın halka bölgesindeki akış koşullarını temsil eden ayrı bir gevşek dolgulu yatak düzeneğinde yapılmıştır. Eksenel konum, konik açı, yatak boyutu ve parçacık yoğunluğunun gaz hız profilleri üzerindeki etkileri incelenmiştir. Halka bölgesinden geçen hava miktarının eksenel mesafe ve parçacık yoğunluğu arttıkça artarken, konik açı arttıkça azaldığı gösterilmiştir. Gazın halka bölgesine dağılması, büyük ölçekli ünitede küçük ölçekli üniteye göre önemli ölçüde daha yüksek bulunmuştur.

Küçük ölçekli konik tabanlı taşkın yataklarda geçekleştirilen lokal gaz hızı ölçümleri, konik tabanlı taşkın yatakların gaz karışım karakteristiğini ölçmek için bir gaz karışımı modelinde kullanılmıştır. Gaz karışım modelini çözmek için bir MATLAB kodu geliştirilmiş ve tüm çalışma koşulları için gaz dağılım katsayıları

hesaplanmıştır. Sonuçlar, bu çalışmada elde edilen dağılım katsayılarının 10^{-2} mertebesine sahip olduğunu ve sabit yatakların dağılım katsayılarından yüksek, akışkan yatakların dağılım katsayılarından düşük ve silindirik taşkın yataklar ile benzer olduğunu göstermektedir. Ek olarak, Peclet sayısı ağır parçacıklara kıyasla hafif parçacıklar için konvektif transferin aksiyel dağılımdan daha dominant olduğunu ortaya koyan 0.56-7.84 aralığında bulunmuştur.

Tüm sonuçlar mevcut korelasyonlarla karşılaştırılmış ve hem yerel gaz hızları hem de dağılım katsayısı için korelasyonların yüksek yoğunluklu parçacıklar için geçerli olmadığı kanıtlanmıştır.

Anahtar Kelimeler: Konik Tabanlı Taşkın Yatak, Yüksek Yoğunluklu Parçacıklar, Lokal Gaz Hızı, Pitot Tüpü, Gaz Dağılım Katsayısı

Dedication to My Beloved Family…

ACKNOWLEDGMENTS

I would like to thank sincerely to my supervisor Prof. Dr. Görkem Külah and I would like to express my gratitude to Prof. Dr. Murat Köksal for their guidance, support, suggestions and more importantly, motivation throughout this study.

I would like to give my special thanks to our invaluable technician, Hasan Çelikli, for his aids, technical supports and friendship.

I extend my gratitude to my colleagues Mehmet Soner Yaşar, Özge Batır, Berkan Atman, Burak Akdeniz, Ezgi Altıntaş and Zeynep Öztan for their advices and precious friendships in this study.

Lastly, I feel the deepest gratitude and send my best thanks to my husband Ali Can Doğan and each and every member of my family, for their encouragement, endless support and love throughout my thesis.

This study was supported by the Scientific and Technological Research Council of Turkey (TUBITAK) as project numbered '115M392'.

TABLE OF CONTENTS

ABSTRACT iii

ÖZ vii

ACKNOWLEDGMENTS x

TABLE OF CONTENTS xi

LIST OF TABLES xiv

LIST OF FIGURES xv

LIST OF ABBREVIATIONS xix

LIST OF SYMBOLS xx

CHAPTERS

1 INTRODUCTION 1

2 GAS VELOCITY DISTRIBUTIONS IN CONICAL SPOUTED BEDS 7

2.1 Literature Survey 7

2.2 Experimental Set-up 12

2.2.1 Materials 14

2.3 Measurement System for Gas Velocity Studies 15

2.3.1 Calibration of the Pitot tube for the Annulus Measurements 16

2.4 Result and Discussion on Gas Velocity Studies 19

2.4.1 Symmetry and Repeatability Experiments 22

2.4.2 Effect of Axial Position 25

2.4.3 Effect of Conical Angle 28

2.4.4 Effect of Bed Size and Particle Density ... 30
2.5 Conclusion ... 32
3 GAS MIXING IN CONICAL SPOUTED BEDS ... 33
3.1 Literature Survey ... 33
3.2 Measurement System for Gas Mixing Studies ... 39
3.3 Gas Mixing Model for Conical Spouted Beds ... 42
3.4 Data Processing and Solution of the Model ... 45
3.4.1 Determination of the measurement points ... 45
3.4.2 Smoothing of the experimental data ... 47
3.4.3 Determination of the boundary condition at the inlet of the streamtubes 49
3.4.4 Developed Model ... 50
3.5 Results & Discussion ... 52
3.5.1 Repeatability Experiments ... 52
3.5.2 Gas Mixing Experiments ... 56
3.6 Conclusion ... 65
4 CONCLUSIONS & RECOMMENDATIONS ... 67
4.1 Conclusion ... 67
4.2 Recommendations ... 69
REFERENCES ... 71
APPENDICES ... 75
A. LabVIEW code for pressure measurement ... 75
B. Determination of the voidage profile of conical spouted beds ... 76
C. LabVIEW code for concentration measurements ... 77

D. Dimensions of the systems 78

E. Sample Calculation: 60^o small scale conical spouted bed operating with zirconia particles 80

LIST OF TABLES

TABLES

Table 2.1 Summary of gas flow studies in spouted beds the literature 8

Table 2.1 Summary of gas flow studies in spouted beds the literature (Continued) 9

Table 2.2 Geometric parameters of the spouted beds 14

Table 2.3 Particle properties 15

Table 2.4 Information of the operating conditions with bed and particle properties 22

Table 2.5 Percentages of air flow amounts through spout, interface, and annulus regions 27

Table 2.6 Percentages of air flow amounts through spout, interface, and annulus regions 30

Table 2.7 Percentages of air flow amounts through spout, interface, and annulus regions 30

Table 3.1 Summary of gas mixing studies in the literature 35

Table 3.1 Summary of gas mixing studies in the literature (Continued) 36

Table 3.2 Operating conditions of the gas mixing experiments 56

Table 3.3 The dispersion coefficients predicted by the gas mixing model and calculated ones with San Jose et al.'s correlation 63

Table 3.4 Peclet numbers for all experimental conditions...................................... 65

LIST OF FIGURES

FIGURES

Figure 1.1 Conical cylindrical spouted bed (Ali et al.,2016) 2
Figure 1.2 Conical spouted bed (Elordi et al., 2007) 3
Figure 1.3 Scope of the hydrodynamic studies 4
Figure 2.1 Photographs of (a) 30º (small), (b) 60º (small), (c) 66º conical beds (large) 13
Figure 2.2 Geometric illustration of the conical spouted beds 13
Figure 2.3 Photographs of the particles (a) zirconia, (b) alumina, (c) glass beads 15
Figure 2.4 The set-up used for calibration of the Pitot tube for annulus measurements... 17
Figure 2.5 Comparison of the measured interstitial gas velocity before and after calibration for the zirconia particles 18
Figure 2.6 Correlation between the interstitial velocity and pressure drop for all particles 19
Figure 2.7 Symmetry experiment for alumina particles (d_p=1 mm, γ=66°, H_b=144 mm, U_0=1.05U_{ms})... 23
Figure 2.8 Repeatability experiments for (a) zirconia, (b) alumina, (c) glass beads particles (d_p=1 mm, γ=66°, H_b=144 mm, U_0=1.05U_{ms}, H_p/H_b=0.7) 24
Figure 2.9 Radial profile of interstitial velocity for zirconia particles (a) spout and interface region; (b) annulus region (d_p=1 mm, γ=60°, H_b=100 mm, U_0=1.25U_{ms})25
Figure 2.10 Radial profiles of interstitial velocity for (a) zirconia, (b) alumina, (c) glass beads particles (d_p=1 mm, γ=60°, H_b=100 mm, U_0=1.25U_{ms})...................... 26
Figure 2.11 Comparison of interstitial gas velocity obtained from San Jose's correlation and experimental measurements for a) glass beads, b) zirconia particles 28

Figure 2.12 Effect of conical angle on the radial normalized gas velocity profiles for (a) zirconia, (b) glass beads particles (for γ=30°, H_b=180 mm, H_p=115 mm; for γ=60°, H_b=100 mm, H_p=70 mm; U_0=1.25U_{ms}) 29
Figure 2.13 Effect of bed size on the radial normalized gas velocity profiles for (a) zirconia, (b) glass beads particles (for large scale unit γ=66°, D_c=250 mm, H_b=144 mm, U_0=1.05U_{ms} ; for small scale unit γ=60°, D_c=150 mm, H_b=100 mm, U_0=1.25U_{ms} ; H_p/H_b=0.5) 31
Figure 3.1 Tracer concentrations in real reactors by using (a) pulse, (b) step functions (Davis and Davis, 2003) 34
Figure 3.2 Photograph of the gas concentration measurement system.................. 40
Figure 3.3 Instrumentation diagram of the measurement system.......................... 41
Figure 3.4 Gas mixing model 43
Figure 3.5 Node numbering.. 47
Figure 3.6 Resulting curves over experimental data taken from (a) the inlet (z=0 mm) and (b) the exit (z=100 mm) (ρ_p=2460 kg/m^3, d_p=1 mm, γ=60°, H_b=100 mm, U_0=1.25U_{ms}) 48
Figure 3.7 Comparison of the measured tracer concentration profiles at the inlet (ρ_p=6050 kg/m^3, d_p=1 mm, γ=30°, H_b=180 mm, z=0 mm, U_0=1.25U_{ms}) 50
Figure 3.8 Repeatability experiments for of zirconia particles at different radial positions (a) r=0 mm, (b) r=3.8 mm (Node 13), (c) r=11.2 mm (Node 14), (d) r=22.9 mm (Node 12), (e) r=39.2 mm (Node 9), (f) r=57.3 mm (Node 5) (ρ_p=6050 kg/m^3, d_p=1 mm, γ=60°, H_b=100 mm, U_0=1.25U_{ms})... 53
Figure 3.9 Repeatability experiments for of alumina particles at different radial positions (a) r=0 mm, (b) r=3.8 mm (Node 13), (c) r=11.2 mm (Node 14), (d) r=22.9 mm (Node 12), (e) r=39.2 mm (Node 9), (f) r=57.3 mm (Node 5) (ρ_p=3700 kg/m^3, d_p=1 mm, γ=60°, H_b=100 mm, U_0=1.25U_{ms})... 54
Figure 3.10 Repeatability experiments for of glass beads particles at different radial positions (a) r=0 mm, (b) r=3.8 mm (Node 13), (c) r=11.2 mm (Node 14), (d)

r=22.9 mm (Node 12), (e) r=39.2 mm (Node 9), (f) r=57.3 mm (Node 5) (ρ_p=2460 kg/m^3, d_p=1 mm, γ=60°, H_b=100 mm, U_0=1.25U_{ms}) 55

Figure 3.11 Comparison of experimental and predicted tracer concentration profiles at different radial positions (a) r=3.8 mm (Node 13), (b) r=11.2 mm (Node 14), (c) r=22.9 mm (Node 12), (d) r=39.2 mm (Node 9), (e) r=57.3 mm (Node 5), (f) experimental tracer profiles (ρ_p=6050 kg/m^3, d_p=1 mm, γ=60°, H_b=100 mm, U_0=1.25U_{ms}, D=0.0608 m^2/s)... 57

Figure 3.12 Comparison of experimental and predicted tracer concentration profiles at different radial positions (a) r=3.8 mm (Node 13), (b) r=11.2 mm (Node 14), (c) r=22.9 mm (Node 12), (d) r=39.2 mm (Node 9), (e) r=57.3 mm (Node 5), (f) experimental tracer profiles (ρ_p=3700 kg/m^3, d_p=1 mm, γ=60°, H_b=100 mm, U_0=1.25U_{ms}, D=0.0469 m^2/s)... 58

Figure 3.13 Comparison of experimental and predicted tracer concentration profiles at different radial positions (a) r=3.8 mm (Node 13), (b) r=11.2 mm (Node 14), (c) r=22.9 mm (Node 12), (d) r=39.2 mm (Node 9), (e) r=57.3 mm (Node 5), (f) experimental tracer profiles (ρ_p=2460 kg/m^3, d_p=1 mm, γ=60°, H_b=100 mm, U_0=1.25$_{Ums}$, D=0.0175 m^2/s) 59

Figure 3.14 Comparison of experimental and predicted tracer concentration profiles at different radial positions (a) r=3.8 mm (Node 13), (b) r=10.9 mm (Node 14), (c) r=21.5 mm (Node 12), (d) r=36.0 mm (Node 9), (e) r=51.2 mm (Node 5), (f) experimental tracer profiles (ρ_p=6050 kg/m^3, d_p=1 mm, γ=30°, H_b=180 mm, U_0=1.25U_{ms}, D=0.0935 m^2/s).. 60

Figure 3.15 Comparison of experimental and predicted tracer concentration profiles at different radial positions (a) r=3.8 mm (Node 13), (b) r=10.9 mm (Node 14), (c) r=21.5 mm (Node 12), (d) r=36.0 mm (Node 9), (e) r=51.2 mm (Node 5), (f) experimental tracer profiles (ρ_p=2460 kg/m^3, d_p=1 mm, γ=30°, H_b=180 mm, U_0=1.25U_{ms}, D=0.0186 m^2/s).. 61

Figure 3.16 Comparison of the dispersion coefficients with literature.................. 64

Figure A.1 LabVIEW code for pressure measurement 75
Figure C.1 LabVIEW code for concentration measurements**Error! Bookmark not defined.**
Figure D.1 30^o small scale bed dimensions .... **Error! Bookmark not defined.**
Figure E.1 Experimental data of exit of the streamtubes (ρ_p=6050 kg/m^3, d_p=1 mm, γ=60°, H_b=100 mm, U_0=1.25U_{ms}) .... **Error! Bookmark not defined.**
Figure E.2 Interstitial velocity change on axial position in spout (ρ_p=6050 kg/m^3, d_p=1 mm, γ=60°, H_b=100 mm, U_0=1.25U_{ms}) .... **Error! Bookmark not defined.**

LIST OF ABBREVIATIONS

ABBREVIATIONS	
BDF	Backward Differentiation Formula
CFD	Computational Fluid Dynamics
CVD	Chemical Vapor Deposition
DAE	Differential Algebraic Equation
HTR	High Temperature Gas Cooled Nuclear Reactors
NDIR	Non-Dispersive Infrared
NDF	Numerical Differentiation Formula
ODE	Ordinary Differential Equation
PDE	Partial Differential Equation
RTD	Residence Time Distribution
TRISO	Tristructural-isotropic type fuel element

LIST OF SYMBOLS

SYMBOLS

Ar	Archimedes number, $gd_p^3(\rho_p-\rho_f)/\mu^2$, -
A_A, A_S	Cross sectional area of annulus and spout, respectively, m^2
C_A, C_S	Tracer concentration in the annulus and in the spout, respectively, -
d_p	Particle diameter, m
D	Dispersion coefficient, m^2/s
D_b	Diameter at the static bed height, mm
D_o, D_c, D_i	Cone bottom, column and gas-inlet diameter, respectively, mm
g	Gravitational acceleration, m^2/s
H_b, H_c, H_p	Height of the static bed height, of the conical section and of measurement port, respectively, mm
L	Characteristic length, m
Pe	Peclet number
Q_J	Gas flow rate, m^3/s
Q_S	Gas flow rate in spout, m^3/s
r	Radial position, mm
r_b	Radius of the bed surface, mm
r_s	Spout radius, mm

U_i, U_0	Interstitial and superficial gas velocity, respectively, m/s
U_{ij}	Interstitial gas velocity at the ij volume element at the interface, m/s
U_{ms}	Minimum spouting gas velocity, m/s
$\overline{U_S}$	Interstitial velocity in the spout at z level, m/s
V	Measured voltage signal, volt
t	time, s
z	Longitudinal coordinate, m

Greek Letters

ΔP	Bed pressure drop, Pa
α	Imaginary cone angle, degree
γ	Angle of the conical section, degree
ε_A, ε_0, ε_S	Bed voidage of annulus, loosely packed and of spout, respectively, -
$\varepsilon(0)$	Bed voidage at the spout center, -
$\varepsilon(w)$	Bed voidage at the wall, -
μ	Gas viscosity, kg/m.s
ρ, θ	Spherical coordinates, longitudinal and angular, respectively
ρ_f, ρ_p	Density of fluid and particle, respectively, kg/m^3
φ	Sphericity

CHAPTER 1

INTRODUCTION

Fluidization in multiphase systems is one of the most preferred operations due to its unusual characteristic features of contacting in industrial applications. Rapid and well mixing, ease of handling and controllable operations, being suitable for large-scale operations and circulation availability are main virtues of fluidized beds. Besides of these motives to prefer, fluidized beds are unfavorable for handling Group D particles according to Geldart classification, which are coarse and dense particles. Enormous amount of fluidizing gas is required to fluidize this type of particles in conventional fluidized beds and this leads to high pressure drops especially at the distributor plates used at gas inlet to the bed. Large bubbles may form and cause slugging (Kunii and Levenspiel, 1991).

As an alternative method for slugging fluidized beds, a new approach named as 'Spouted Bed' was developed in 1954 by Gishler and Mathur at the National Research Council of Canada. In spouted bed which is a vessel with generally conical base to eliminate the dead zones filled with coarse particles, spouting gas is introduced vertically from the central part of the base with a nozzle. Three distinct regions are constituted: spout, fountain and annulus as shown in Figure 1.1. When spouting gas is injected to the system with sufficiently high flow rate, the introduced gas creates a dilute region called 'spout' and pushes the particles towards the surface of the bed and forms a 'fountain'. These particles fall back via gravity to dense region called 'annulus' between the internal jet and the bed wall. As the spouting fluid flows upward, it penetrates through the annulus region. That makes annulus a loosely packed section. As the introduced gas goes up, particles descend. Particles at the surface of the bed travel with a slow motion towards downward and affiliate to the flow. That is the complete circulation (Epstein and Grace, 2011).

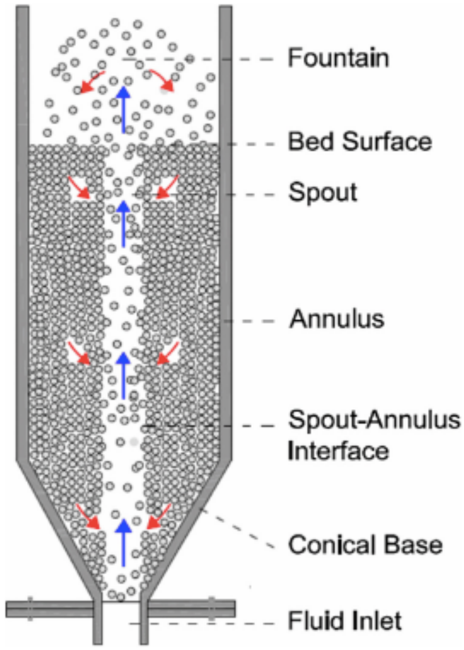

Figure 1.1 Conical cylindrical spouted bed (Ali et al.,2016)

Owing to cyclic movement of the solid particles which is a unique characteristic of spouted beds, use of spouted beds which started with drying of moist wheat particles was expanded to many applications such as combustion, gasification, pyrolysis, polymerization, particle coating and chemical vapor deposition (Kunii and Levenspiel, 1991). In some of these applications, residence time of the gaseous phase has crucial importance and is desired to be optimum. For fast reactions, it should be as short as possible such as a few milliseconds (Stocker et al., 1989). Cylindrical bed wall with conical base which is the conventional geometry of spouted beds are seen to be inconvenient to provide this optimum residence time of the gas. In addition, gas-solid contact is limited in the annulus region because of the dead zones. To eliminate these disadvantages, conical spouted beds, shown in Figure 1.2, are proposed. Considering the particles are only in conical section, conical spouted beds have the potential to minimize dead zones and the gas residence time.

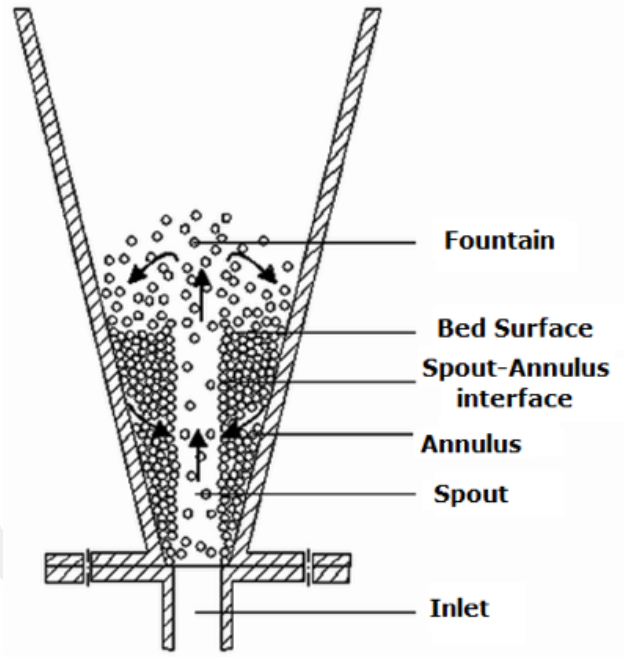

Figure 1.2 Conical spouted bed (Elordi et al., 2007)

To properly design and operate the conical spouted beds, first the hydrodynamic properties of the bed must be known. The fundamental hydrodynamic studies of spouted beds cover the topics shown in Figure 1.3 below.

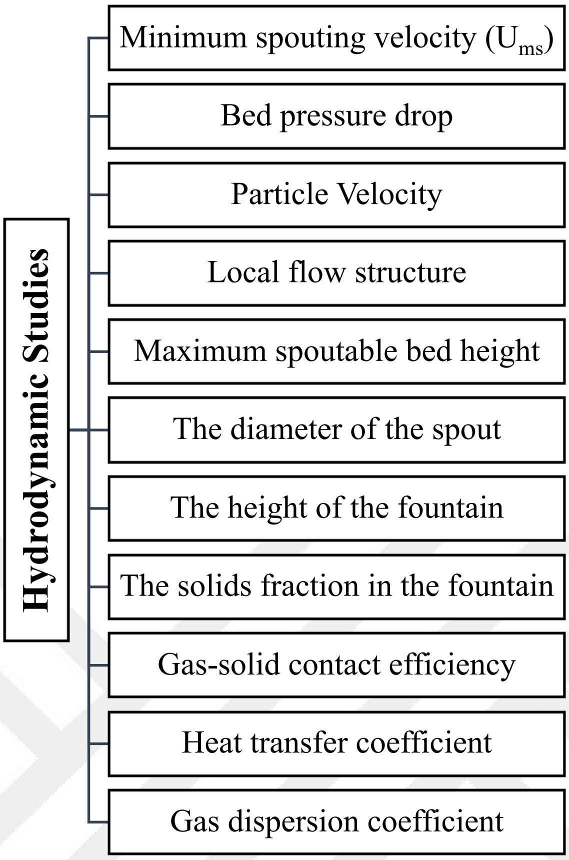

Figure 1.3 Scope of the hydrodynamic studies

The hydrodynamic behavior of the system mainly depends on the design parameters and operating conditions of the conical spouted bed such as bed geometry, particle diameter, particle density, inlet gas flow rate and static bed height. Consequently, the hydrodynamics of conical spouted beds was found to be different from the conical cylindrical spouted beds. (Mathur and Epstein, 1974, Olazar et al., 1992)

Conical spouted beds have been used in applications such as drying, catalytic polymerization, treatment of wastes, particle coating and chemical vapor deposition (Epstein and Grace, 2011). Because of their unique gas-solid contact characteristics, these systems have been especially favored for the coating of uranium dioxide kernels with pyrolytic carbon and silicon carbide to produce spherical tristructural-isotropic (TRISO) type fuel elements through chemical vapor deposition (CVD) technique. One important characteristics of this process is that during coating, the density of uranium dioxide particle decreases from 10000 to 2500 kg/m^3 resulting in an average particle density of 6000 kg/m^3 that is higher than that of typical particles processed in spouted beds. TRISO type fuel elements are being planned to be used in next generation very high temperature gas cooled nuclear reactors (HTR) which require qualified perfectly coated fuel particles for safety (Sari et al., 2012). Since this advance reactor technology is still under development, TRISO particles are used in the prototype reactors and produced in small-scale spouted bed coaters. Once the full-scale reactors are in operation, need for large-scale CVD spouted bed coaters will be eminent. Therefore, detailed understanding of the hydrodynamics of the conical spouted beds is of essential importance for successful design and scale up of these coaters (Kulah et al., 2016).

Although considerable number of studies on hydrodynamics of conical spouted beds are available in the literature (Thorley et al., 1959, Becker, 1961, Mamuro and Hattori, 1968, Van Velzen et al., 1972, Mathur and Epstein, 1974, Lim and Mathur, 1976, Olazar et al., 1992, Olazar et al., 1995, San Jose et al., 1995, Bi et al., 1997, Olazar et al., 2001, Lu et al., 2001, San Jose et al., 2005, Wang et al., 2006, Epstein and Grace, 2011, Kulah et al., 2016) , studies conducted in spouted beds operating with heavy particles (ρ_p >2500 kg/m^3) (Sari et al., 2012, Zhou, 2008, Mostoufi et al., 2015, Rojas, 2010, Ali et al., 2016, Aradhya et al., 2017) are limited and these studies are mainly focused on the determination of the minimum spouting velocity, time-averaged and dynamic pressure drops, fountain height, particle velocity and solids hold-up (Kulah et al., 2016). For complete characterization of conical spouted beds, determination of the local flow structure based on gas velocity and gas mixing is of paramount importance. However, as will be elucidated in detail in Chapter 2 and 3 of this thesis, there are limited studies on local gas behavior in conical spouted beds, especially operating with high-density particles. Therefore, the objective of this thesis study was to investigate the effect of particle density, bed size, conical angle on the local gas behavior and the gas mixing behavior in conical spouted beds.

CHAPTER 2

GAS VELOCITY DISTRIBUTIONS IN CONICAL SPOUTED BEDS

2.1 Literature Survey

The determination of the gas flow structure and gas mixing behavior of the conical spouted beds has crucial significance on the characterization of conical spouted beds. The flow pattern of the gas can shed light on gas mixing phenomenon, which is a crucial aspect in reactor design. The gas dispersion within the spouted beds is a complex subject that is not fully enlightened due to the difficulties of determining the local gas velocity distribution. To properly model the gas dispersion in spouted beds, exact flow structure must be investigated. The gas velocity profiles can also be used to validate the results of the computational fluid dynamics (CFD) studies (Wang, 2006). Gas flow studies in spouted beds are summarized in Table 2.1. The only study of the gas velocity conducted in spouted beds operating with heavy particles (ρ_p>2500 kg/m^3) was presented by Zhou (2008). Despite these studies, the investigation of gas velocity in spouted beds operating with light particles is quite limited in the literature.

Table 2.1 Summary of gas flow studies in spouted beds the literature

AUTHORS	PARTICLE PROPERTIES			BED PROPERTIES				BED TYPE	METHOD
	Type	d_p (mm)	ρ_p (kg/m^3)	γ	D_c (mm)	H_c (mm)	H_b (mm)		
Thorley et al. (1959)	Wheat	3.7	830	45 60 85	152 305 610	-	305-1850	Conical cylindrical spouted bed	Static pressure measurement from the wall
Becker (1961)	Wheat	3.38	1378	45 60	152 229	-	-	Conical cylindrical spouted bed	Pitot tube measurement
Mamuro and Hattori (1968)	Wheat Soma-sand	2.8 1.18	1350 2610	60	150	127	190-340	Conical cylindrical spouted bed	Pitot tube measurement
Van Velzen et al. (1972)	Zirconium oxide Glass Glass Permutit Polystyrene Polystyrene	0.590-0.850 0.745-0.890 0.890-1.22 0.590-0.840 0.500-0.700 1-1.32	4400 2600 2600 1600 1000 1000	31	125	170	50-300	Conical cylindrical spouted bed	Prandtl tube measurement
Lim & Mathur (1974)	Wheat Polystyrene	3.45 2.67	1177 1020	60	152	-	457 305 152	Conical cylindrical spouted bed	Static pressure measurement for annulus; Pitot tube measurement for spout

Table 2.2 Summary of gas flow studies in spouted beds the literature (Continued)

AUTHORS	PARTICLE PROPERTIES			BED PROPERTIES				BED TYPE	METHOD
	Type	d_p (mm)	ρ_p (kg/m^3)	γ	D_c (mm)	H_c (mm)	H_b (mm)		
Lim & Mathur (1976)	Polystyrene Polystyrene Wheat Millet Glass beads Glass beads Ammonium nitrate Ammonium nitrate	2.93 1.61 3.50 2.15 2.93 1.10 1.99 1.45	1050 1050 1240 1180 2940 2960 1750 1740	60	152 241 292	-	-	Conical cylindrical spouted bed	Static pressure measurement for annulus; Pitot tube measurement for spout
Olazar et al. (1995)	Expanded polystyrene	3.5	14	45	50	360	280	Conical spouted bed	Prandlt tube measurement
San Jose et al. (1995)	Glass spheres Extruded polystyrene Rice	1-2-3-4-6-8 4.1 3.8	2240 960 1250	45 39 36 33 28	360	360 400 450 500 600	100-340	Conical spouted bed	Pitot tube measurement
Zhou (2008)	Yttrium-stabilized zirconia	0.5	5890	60	50	35	35	Conical spouted bed	Pitot tube measurement

Two different methods have been generally used to determine the gas velocity profiles in spouted beds (Mathur and Epstein, 1974). In the first method, the gas velocity is calculated from the static pressure drop change in the axial direction measured at different axial heights on the bed wall. Thorley et al. (1959) applied this method to obtain an average velocity value for the annulus section of the conical cylindrical spouted bed having conical angles of 45^o, 60^o and 85^o using wheat particles (ρ_{wheat}=830 kg/m^3). To convert the pressure data to gas velocity, they conducted experiments by using a moving packed bed at the same operating conditions. Using the results obtained from both systems, gas velocity versus pressure drop at unit height was plotted. These plots were compatible with the axial pressure drop measurements carried out on the bed wall, and therefore, were related to the gas velocity in annulus zone. The air flow in the spout region was calculated from the difference between total air flow and air flow through the annulus.

In the second method, the local gas velocity is measured with a Pitot tube or a Prandtl tube. Although Pitot tube is a robust and easy to use device, the use of data obtained by Pitot tube in multiphase systems is very complex.

Becker (1961) and Mamuro and Hattori (1968) measured the local gas velocities both in the spout and the annulus sections and reported the results of direct Pitot tube measurements. Mamuro and Hattori (1968) conducted experiments in full and half column spouted beds having 15 cm ID and a conical angle of 60^o operating with wheat and soma-sand particles (ρ_{wheat}=1350, ρ_{sand} =2610 kg/m^3). The measurements were taken from the cylindrical part of the bed. It was observed that the local gas velocity was the highest near the gas injection in the spout zone and decreased towards the annulus zone. A half column was used for the determination of the diameter of the spout and with this information volumetric flowrate of the gas was calculated from the cross-sectional average of the measured local gas velocity. They found values much higher than the total gas flow fed to the system.

This made the reliability of the measurements, especially the ones taken in the annulus section, debatable. Therefore, they concluded that the local gas velocity measurement done by Pitot tube was only justified for the spout region.

In the study carried out by Van Velzen et al. (1972), a calibrated Prandtl tube was used for the measurements. Even though the measurements were taken from the conical section of the spouted bed, some negative gas velocity values were observed near the gas injection. Therefore, radial gas velocity distribution was not reported.

Lim and Mathur (1974, 1976) carried out measurements in both conical and cylindrical part of the spouted bed having a cone angle of 60^o with various particles (ρ_p = 1020-1750 kg/m^3). To obtain gas velocity, they used static pressure measurement in the annulus region of the cylindrical part of the bed. Because the assumptions are not valid in both conical and the cylindrical sections of the bed as Thorley (1959) reported before, they used a Pitot tube for the measurements in the spout region of the conical part of the bed. The gas flowrate in the unmeasured section (annulus) was determined by subtracting the measured flowrate from the total flowrate (Thorley et al., 1959, Mamuro and Hattori, 1968, Lim and Mathur, 1976).

The most recent studies were carried out by one of the most active groups at University of the Basque Country, Spain in this field. Olazar and co-workers used a Prandtl tube to measure gas velocity both in the spout and the annulus region of the spouted bed having 45^o cone angle with expanded polystyrene particles ($\rho_{polystyrene}$ =14 kg/m^3) in their first study in 1995. Based on the experimental results, they proposed a correlation for local gas velocity as a function of radius, maximum velocity, minimum velocity and height by fitting the experimental data to a Gaussian curve. Then, San Jose et al. (1995) expanded their study by applying same method of approach. Spouted beds having different cone angles (45^o, 39^o, 36^o, 33^o, 28^o) with glass beads, extruded polystyrene and rice particles (ρ_{glass}=2420, $\rho_{polystyrene}$ =960, ρ_{rice} =1250 kg/m^3) were used. In this study, more than 900 experimental results were analyzed, and vertical component of gas velocity correlation obtained before (Olazar et al., 1995) was improved. This empirical correlation of the velocity is the only one in the literature and was obtained by using the gas velocity measurements carried out with light particles ($\rho_p < 2500$ kg/m^3). Although this study is most comprehensive one, no information was given regarding how the Prandtl tube was calibrated if it was or no comment was made whether the measurements in the annulus section can be used directly without calibration.

As can be inferred from the literature, to obtain reliable local gas velocity distributions comprising both the spout and the annulus section of the conical spouted beds, the problems revealed in the previous studies must be properly addressed. Therefore, the objectives of this part of the study were to develop a system that measures the local gas velocities accurately and investigate the change of local flow structure in conical spouted beds operating with both low and high-density particles.

2.2 Experimental Set-up

The gas velocity experiments were conducted in three different conical spouted beds with different conical angles. Two of the spouted beds (30º, 60º) were considered as small scale and the other one (66º) was large scale due their upper column diameter. The illustrations of the conical spouted beds are given in Figure 2.1. The small-scale beds are made of polyoxymethylene and the large scale one is made of carbon steel. All systems have an upper transparent cylinder part.

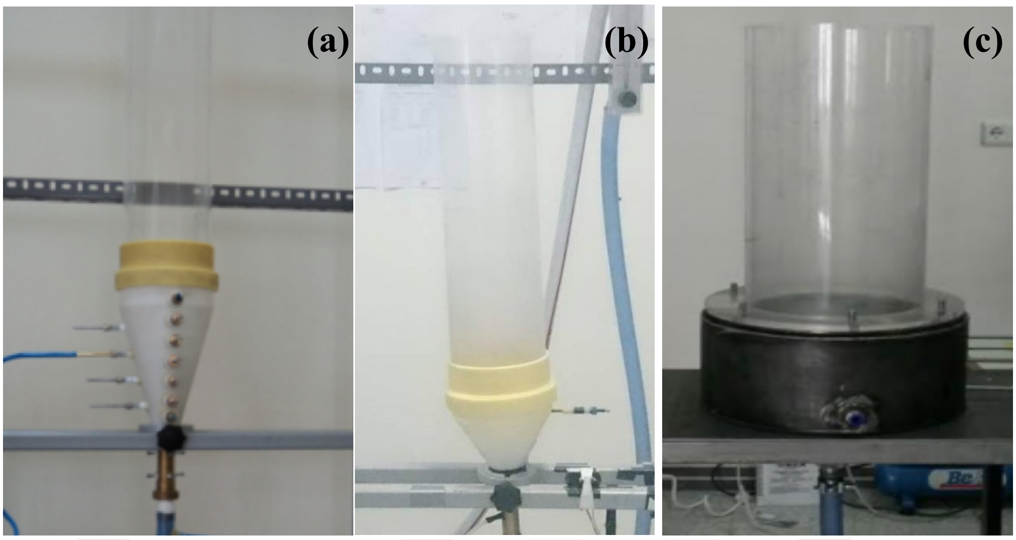

Figure 2.1 Photographs of (a) 30º (small), (b) 60º (small), (c) 66º conical beds (large)

A geometric illustration of the units and geometric parameters are presented in Figure 2.2 and Table 2.2, respectively.

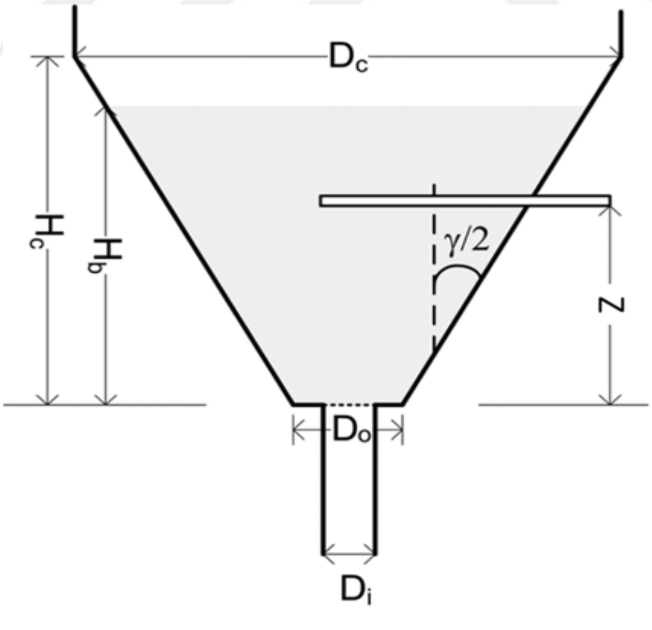

Figure 2.2 Geometric illustration of the conical spouted beds

Table 2.3 Geometric parameters of the spouted beds

Parameters	Small Scale		Large Scale
γ (°)	30°	60°	66°
D_c (mm)	150	150	250
D_o (mm)	25	25	40
D_i (mm)	15	15	15
H_c (mm)	233	108	155
H_b (mm)	180	100	144
$z_{1,2,3}$ (mm)	44, 80, 115, 148	30, 50, 70	50, 72, 100

Compressed air at ambient conditions was used as spouting gas which was supplied from a screw-type compressor at a pressure of 8 bar with 3m^3/min maximum flow rate capacity. To adjust the spouting gas fed to the system, a mass flow controller (MCR-1500SLPM-D/5M, Alicat Scientific) was used. To prevent the possible fluctuations of air flow, two air tanks of 30 L in volume were placed in the supply line.

2.2.1 Materials

Three different spherical particles, which were all 1 mm, were used in this study which are zirconia, zirconia toughened alumina and the glass beads. In addition to low density glass beads, high density particles are also used to analyze the effect of particle density on the hydrodynamics of the system in this study. Illustrations of the particles are given in Figure 2.3 and the properties of the particles are given in Table 2.3, respectively. The loosely packed voidage of the particles (ε_0) were determined by using a graduated cylinder and volumetric calculation.

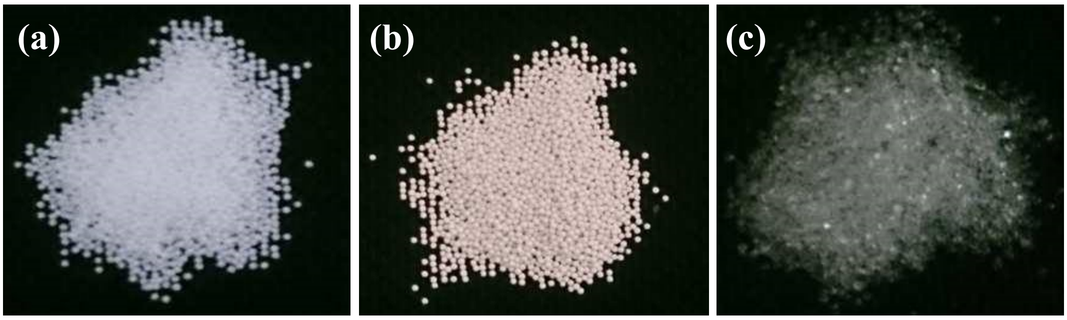

Figure 2.3 Photographs of the particles (a) zirconia, (b) alumina, (c) glass beads

Table 2.4 Particle properties

Particles	**d_p (mm)**	**φ**	**ρ_p (kg/m^3)**	**ε_0**
Glass Beads	1	1	2460	0.36
Alumina (zirconia toughened)	1	≥ 0.95	3700	0.40
Zirconia	1	≥ 0.95	6050	0.38

2.3 Measurement System for Gas Velocity Studies

A "straight" type pitot tube (TPL-D-03-300, KIMO) with an outer diameter of 3 mm and a length of 300 mm made of stainless steel was used to measure the local gas velocities. The tip of the Pitot tube measures total pressure at the measuring point and static pressure is measured by 6 symmetrically positioned holes 25 mm above the tip. The dynamic pressure is calculated from the pressure difference measured between these two locations and the value is converted to velocity with an appropriate calibration equation suggested by the manufacturer as follows:

$$U_i = 1.291 * \sqrt{\Delta P} \tag{2.1}$$

The two lines of the Pitot tube which give the total pressure and static pressure values are connected to the pressure transducer (PX163-120BD5V, OMEGA) to measure the pressure difference. The available operating range of the transducer is -0.02 to

0.11 bar. The output of the pressure transducer is in Volt and the voltage value is converted to pressure by using the calibration equation of the transducer obtained before as follows:

$$\Delta P = 3200.7(V - 1.397) \tag{2.2}$$

The analog voltage signal from the pressure transducer is sent to the data collection card (PCI-6280, NI). LabVIEW software from National Instruments is used to convert data analog-to-digital and control data acquisition. The written code for pressure measurements is given in Appendix A. With this code, 2000 data were recorded at each measurement point. The sampling frequency was 1 kHz.

Since the voidage is very high in the spout ($\varepsilon > 0.75$), it is reasonable to assume that the presence of the particles does not have significant effect on the pitot tube calibration and the single phase calibration equation of the Pitot tube can be used as verified by Mamuro and Hattori (1968). However, for the annulus region, due to nearly loosely packed bed conditions, a new calibration equation is required. Therefore, before the experiments, the Pitot tube was calibrated for the measurements in the annulus section.

2.3.1 Calibration of the Pitot tube for the Annulus Measurements

To obtain the calibration curves, a 78 mm ID cylindrical system shown in Figure 2.4 was used where particles were kept at almost loosely packed condition to simulate the conditions in the annulus section of the spouted bed. The bed material is transparent to observe the flow regime. Pitot tube was located at the center of the cylindrical system and the measurements were taken by inserting the Pitot tube from the exit of the bed vertically.

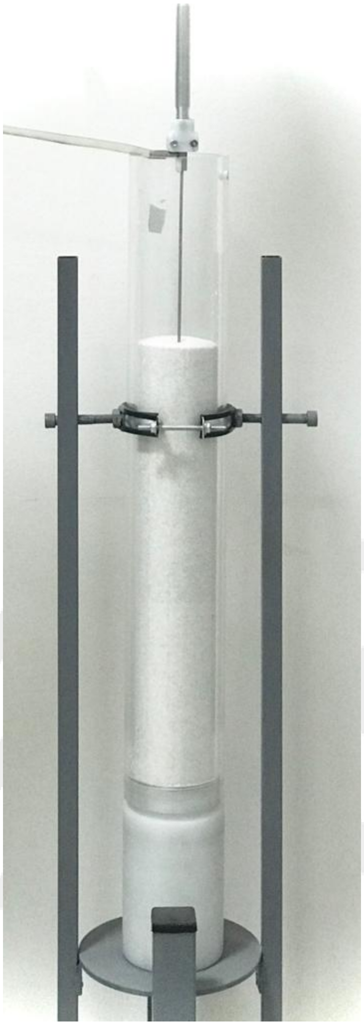

Figure 2.4 The set-up used for calibration of the Pitot tube for annulus measurements

In the previous works conducted in our research group (Kulah et al., 2016, Yeniçeri, 2019), it was found that the voidage in the annulus was almost constant and its average value was found to change approximately by 15% around the loosely packed value. The pressure drop measurements by Pitot tube were taken from the center of the cylindrical system as the radial distribution of the gas velocity in the calibration set-up was found to be flat without significant wall effect supporting the plug flow assumption. Superficial velocities in the cylindrical system were calculated by dividing the air flow measured by using mass flow controller device by the area of the bed. Superficial velocities were converted to the interstitial (local) velocities by using the loosely packed voidage of the particles. The results showed that the local gas velocities calculated using the single phase calibration equation of the Pitot tube supplied by the manufacturer resulted in more than 1300% higher values than the actual local gas velocities which verified the inaccurate results observed in previous studies reported in the literature. An example comparison of the measured local gas velocity before calibration and the calculated local gas velocity after calibration of the zirconia particles is given in Figure 2.5. The calibration curves obtained for all types of particles used in this study are illustrated in Figure 2.6.

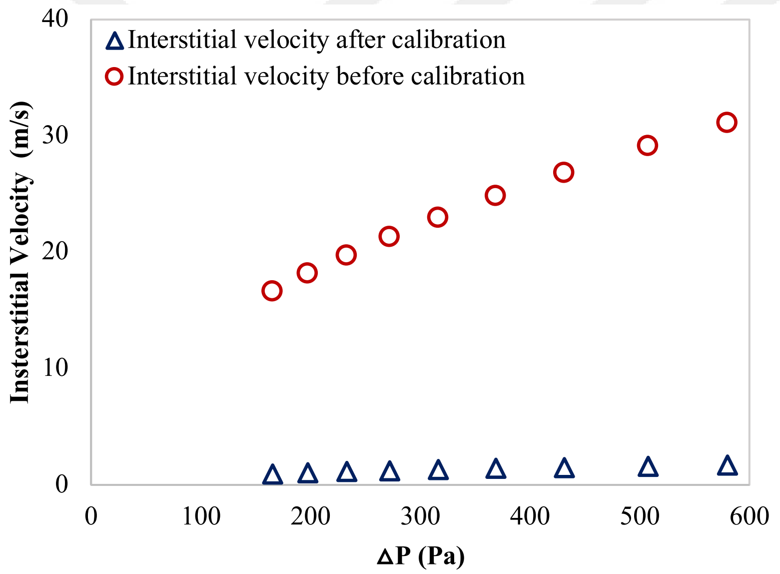

Figure 2.5 Comparison of the measured interstitial gas velocity before and after calibration for the zirconia particles

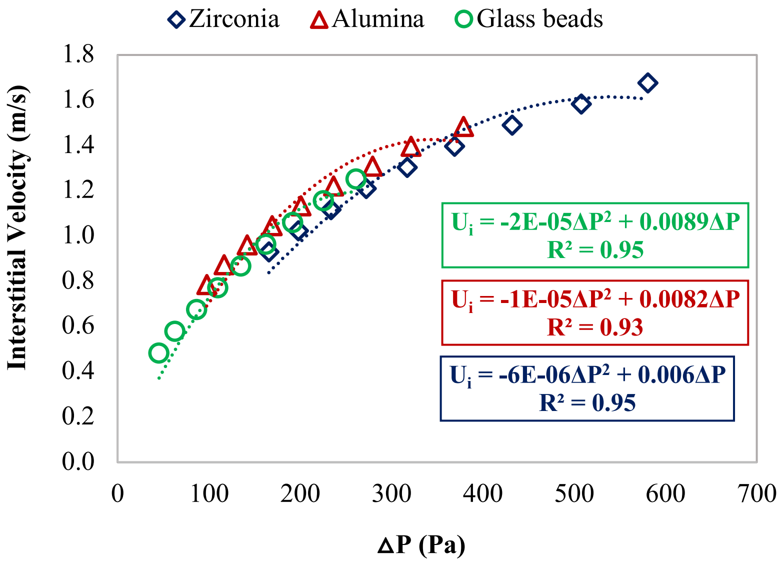

Figure 2.6 Correlation between the interstitial velocity and pressure drop for all particles

2.4 Result and Discussion on Gas Velocity Studies

In the literature, spouted beds are generally divided into two regions: annulus region and spout region which also includes the interface region between spout and annulus. Differently from literature, in this study, spout and interface regions were defined separately. In another study conducted in our research group (Yeniçeri, 2019), radial and axial voidage distributions were measured by using an optical probe and an empirical correlation to predict voidage distribution was developed by modifying the correlation obtained by San Jose et al. (1998) for low and high density particles. the details of this correlation is given in Appendix B. In that study, the spout was defined as the region where voidage was almost constant and it was found to be approximately equal to the gas inlet diameter. Correspondingly, in this study, spout was defined as the region where voidage was constant and interface was defined separately from spout.

The flow structure can be represented as both superficial and interstitial gas velocities. Superficial gas velocity is the empty tube velocity and interstitial gas velocity is the velocity when the particles exist within the bed and it can be calculated as follows:

$$U_i = \frac{U_0}{\varepsilon} \tag{2.3}$$

where ε is the voidage in the bed. Superficial gas velocities were calculated by utilizing the empirical correlation developed in our group for local voidage prediction (Yeniçeri, 2019) and amount of air flowing through the spout, interface and annulus was calculated separately by numerical integration of the superficial gas velocities.

Since the calibration equations developed for spout or annulus region cannot be used directly in the interface region, calibration equations of spout and annulus were extended until center of the interface from both sides to calculate the volumetric flow rate of air going through the interface. Measurements for local gas velocities of interface were taken at this point which means that the local gas velocities of the interface were calculated by using distance average of the calibration equations of spout and the annulus regions. When the total amount of air entering the bed was compared with the calculated amount, the discrepancies were found to be in the range of 1-15%, with an average of 7.8%.

Local gas velocities were measured at several radial and axial positions in three different spouted beds. Before the local gas velocity experiments in spouted beds, the minimum stable spouting velocities (U_{ms}), symmetry of the gas flow and repeatability of the results were investigated. Minimum stable spouting velocity means inlet gas velocity at which the external spouting begins. For each case, minimum stable spouting velocities were determined visually by observing the point at spout collapse while the inlet gas velocity decreases gradually to avoid the hysteresis affect. Hysteresis means that the pressure drop measured as the bed regime changes from packed bed to fluidized bed is much higher in the ascending velocity process associated with the strength of interparticle forces. In spouted beds, hysteresis is related with the development of gas cavity and the internal spout (Epstein and Grace, 2011). In all conducted experiments, superficial air velocity was set to 1.25 times of U_{ms} for small scale beds and 1.05 times of U_{ms} for large scale bed to ensure that experiments were performed during stable spouting operation. The Pitot tube was inserted vertically from the top of the column at different axial positions. At each axial location, the probe was also traversed from the wall to the center to obtain radial profile of gas velocities. The measurement locations and operating conditions are presented in Table 2.4.

Table 2.5 Information of the operating conditions with bed and particle properties

Parameters	γ (°)	D_c (mm)	ρ_p (kg/m³)	z (mm)	H_b (mm)	z/H_b	U_{ms} (m/s)	U_0/U_{ms}
Effect of Axial Position	60	150	6050	30 50 70	100	0.3 0.5 0.7	35.4	1.25
	60	150	3700	30 50 70	100	0.3 0.5 0.7	30.2	1.25
	60	150	2460	30 50 70	100	0.3 0.5 0.7	24.1	1.25
Effect of Conical Angle	30	150	6050	115	180	0.64	44.3	1.25
	60	150	6050	70	100	0.70	35.4	1.25
	30	150	2460	115	180	0.64	25.0	1.25
	60	150	2460	70	100	0.70	24.1	1.25
Effect of Solid Density	60	150	6050	50	100	0.50	35.4	1.25
	60	150	2460	50	100	0.50	24.1	1.25
	66	250	6050	72	144	0.50	57.5	1.05
	66	250	2460	72	144	0.50	37.3	1.05

2.4.1 Symmetry and Repeatability Experiments

Symmetry and repeatability experiments were conducted by using 3 different particles for the same operating conditions on different days. The centerline of the conical spouted beds is accepted at r = 0 mm and the measurements were taken by traversing the Pitot tube across the entire diameter of the bed. Figure 2.7 is given as an example to show the radial superficial velocity distributions of alumina particles on different axial positions in 66° conical spouted bed. The results indicate that the gas velocity profile is symmetrical around the spout axis (r = 0). Consequently, the rest of the measurements in this study were taken by traversing the probe from center to the wall, which represents the entire bed profile.

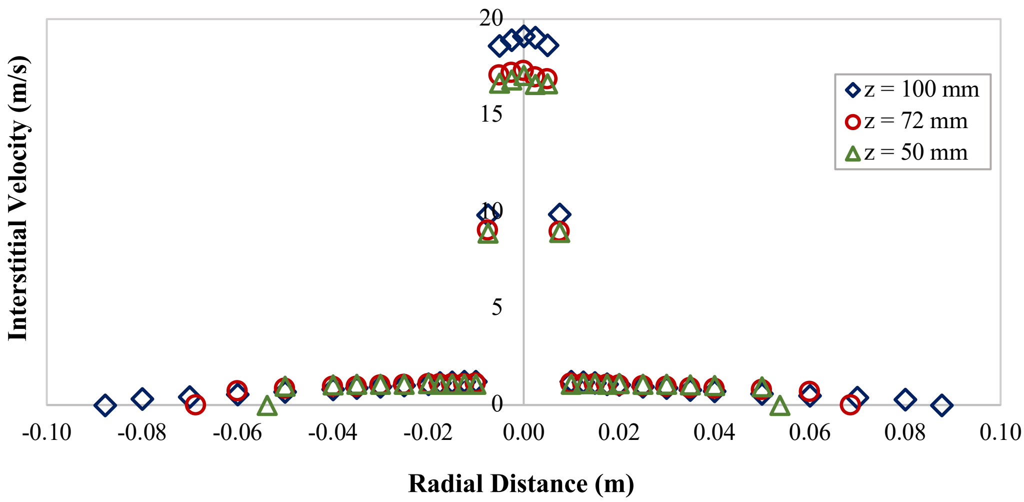

Figure 2.7 Symmetry experiment for alumina particles (d_p=1 mm, γ=66°, H_b=144 mm, U_0=1.05U_{ms})

The aim of the repeatability experiments is to investigate the repeatability of the results independent from the environmental conditions. Figure 2.8 proves that the results are repeatable for all types of particles and under all operating conditions investigated in this study.

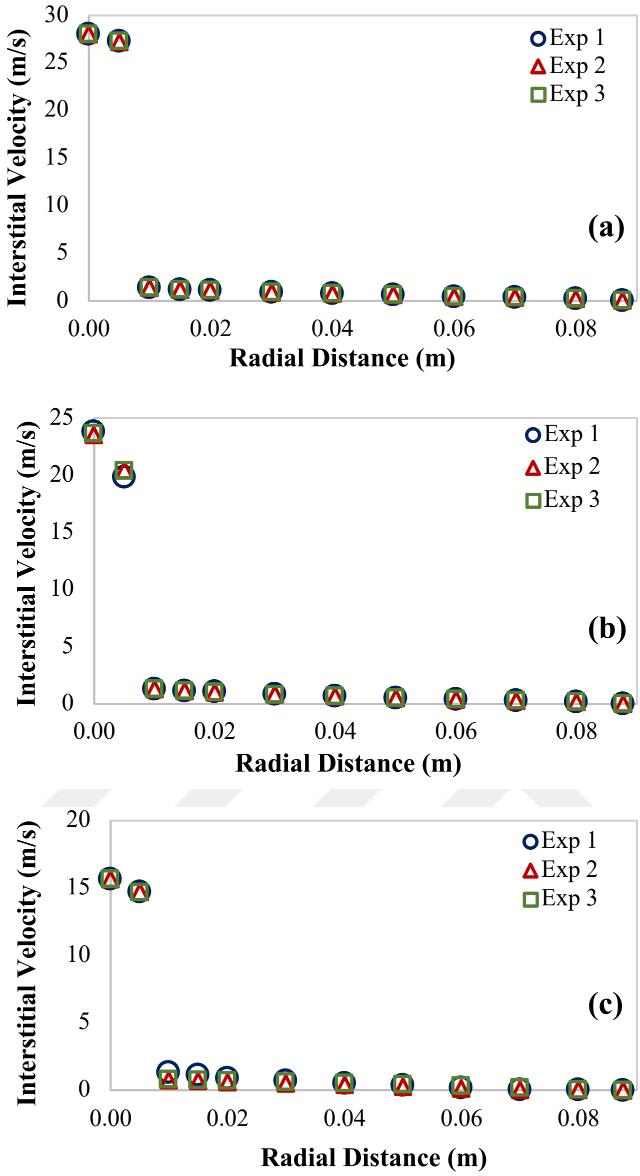

Figure 2.8 Repeatability experiments for (a) zirconia, (b) alumina, (c) glass beads particles (d_p=1 mm, γ=66°, H_b=144 mm, U_0=1.05U_{ms}, H_p/H_b=0.7)

2.4.2 Effect of Axial Position

An example of the change of interstitial gas velocities between the spout, interface, and annulus regions for zirconia particles in the spouted bed having conical angle of 60° is shown in Figure 2.9. To accentuate the change of gas velocities, the interstitial gas velocities of spout and interface are given in Figure 2.9 (a), while the interstitial gas velocities of annulus are given in Figure 2.9 (b). For all conditions, much higher velocities were obtained in the spout region than the annulus region as expected.

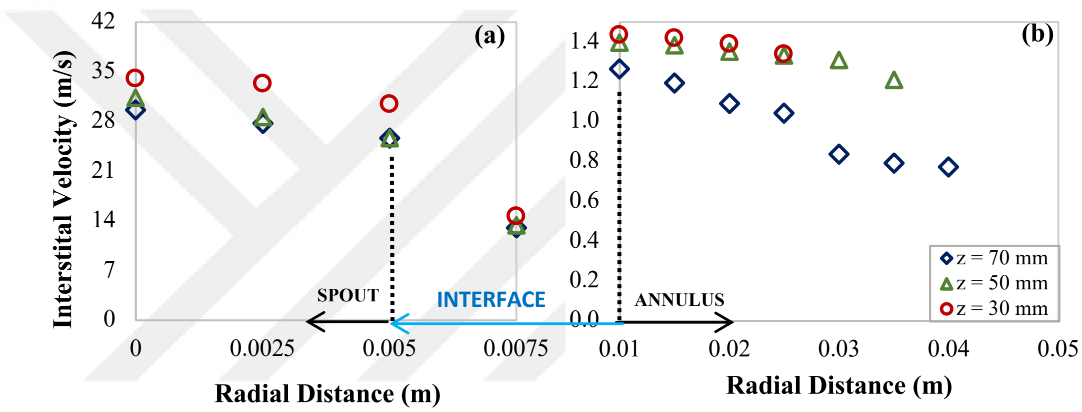

Figure 2.9 Radial profile of interstitial velocity for zirconia particles (a) spout and interface region; (b) annulus region (d_p=1 mm, γ=60°, H_b=100 mm, U_0=1.25U_{ms})

Effect of axial position on the interstitial gas velocities of three different particles measured in the same system is illustrated in Figure 2.10. As depicted in Figure 2.9 and Figure 2.10, the gas velocity decreases with the increase in the axial height for all particles.

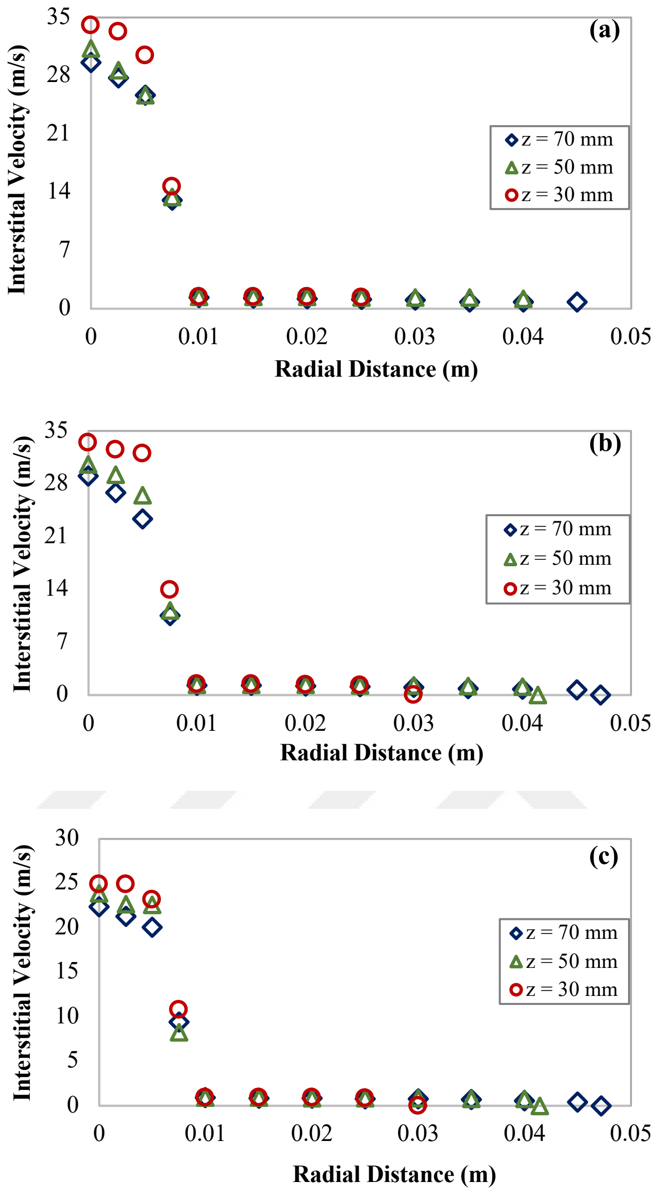

Figure 2.10 Radial profiles of interstitial velocity for (a) zirconia, (b) alumina, (c) glass beads particles (d_p=1 mm, γ=60°, H_b=100 mm, U_0=1.25U_{ms})

The percentages of air flow amount through spout, interface and annulus regions are given in Table 2.5. As can be seen in this table, as the axial distance increases, the amount of air flowing through the annulus increases which means that more gas travels into the annulus at higher parts of the conical spouted bed. It is noteworthy that the amount of air flowing through the interface decreases towards the middle of the bed, then slightly increases towards the bed exit.

Table 2.6 Percentages of air flow amounts through spout, interface, and annulus regions

Parameters	z (mm)	% air flows through spout	% air flows through interface	% air flows through annulus
Zirconia	30	55.1	18.6	26.3
	50	44.7	15.0	40.3
	70	43.3	15.2	41.5
Alumina	30	55.3	17.8	26.9
	50	43.4	13.1	43.5
	70	42.7	13.2	44.1
Glass Beads	30	57.5	18.8	23.7
	50	49.2	12.9	37.9
	70	45.1	14.6	40.3

The only correlation for local gas velocity available in the literature proposed by San Jose et al. (1995) as stated before. A comparison of results obtained from San Jose's correlation and experimental measurements taken from the spout region of the 60^{o} conical spouted bed operating with glass beads and zirconia particles are given in Figure 2.11.

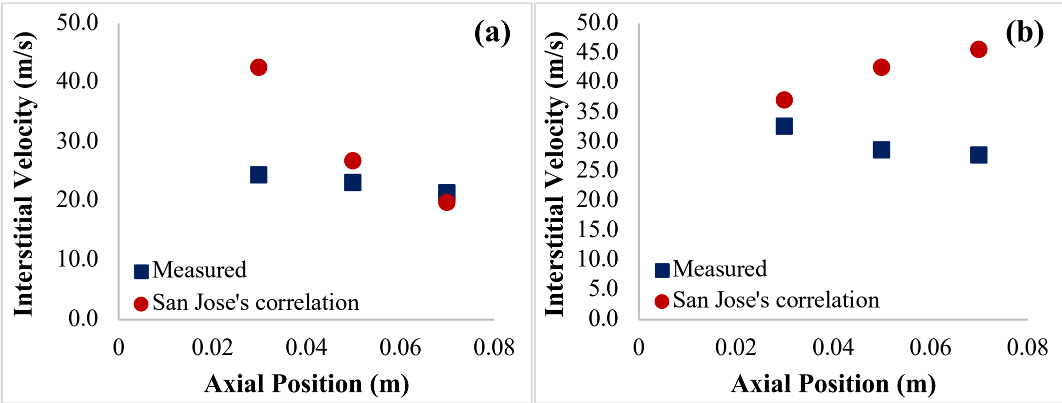

Figure 2.11 Comparison of interstitial gas velocity obtained from San Jose's correlation and experimental measurements for a) glass beads, b) zirconia particles

The results show that the San Jose's correlation gives more satisfactory predictions for glass beads particles. On the other hand, it was found that for particles having higher density than approximately 4130 kg/m^3, as the axial position increases the gas velocity expected to decrease increases according to correlation. This confirms that this correlation is only valid for light particles.

2.4.3 Effect of Conical Angle

Effect of conical angle on the gas velocity profiles for zirconia and glass bead particles in two different spouted beds having conical angles of 30^0 and 60° is illustrated in Figure 2.12. Since the measurement heights in two spouted beds with different conical angle were not equal, the ratio of the measurement height to static bed height was tried to be set close to each other for comparison. Although both systems operated at $U_0 = 1.25U_{ms}$, the minimum spouting velocity increases with static bed height and particle density. As a result, higher local gas velocities are expected for high-density particles in spouted bed having conical angle of 30^0. Therefore, to make a clear comparison, the superficial gas velocities were normalized by dividing it to the minimum spouting velocity in Figure 2.12. As can be seen in Figure 2.12, the difference between the normalized velocities measured in the spout region of the spouted beds with two different cone angles is more significant for light particles than heavy particles. The experiments show that the normalized gas velocities reach higher values in the spout region as the conical angle increases. No significant effect of cone angle on the normalized gas velocities in the annulus region is observed. The effect of cone angle on the percentages of air flow amounts through spout, interface and annulus regions are presented in Table 2.6. It was found that, as the cone angle increases the amount of air that flows through the annulus decreases indicating that gas penetration to the annulus region becomes harder for the spouted beds with wider angle. The slight decrease in the amount of air flowing through the interface region supports this phenomenon.

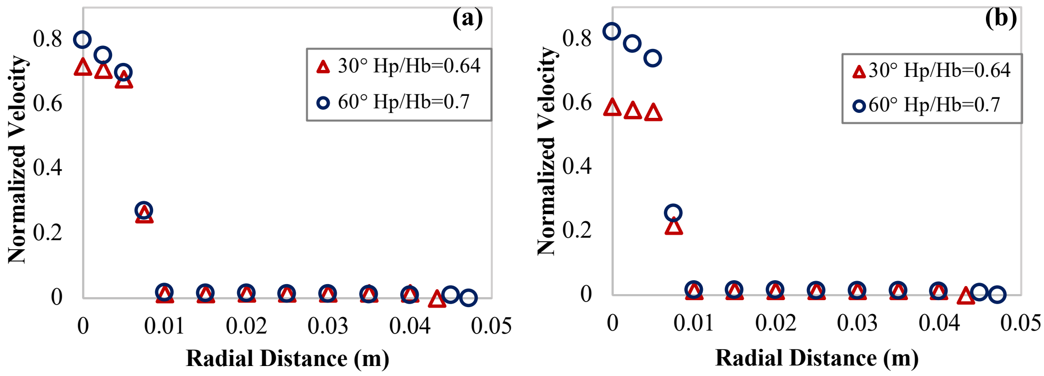

Figure 2.12 Effect of conical angle on the radial normalized gas velocity profiles for (a) zirconia, (b) glass beads particles (for γ=30°, H_b=180 mm, H_p=115 mm; for γ=60°, H_b=100 mm, H_p=70 mm; U_0=1.25U_{ms})

Table 2.7 Percentages of air flow amounts through spout, interface, and annulus regions

Particle	γ (°)	H_p/H_b	% air flows through spout	% air flows through interface	% air flows through annulus
Zirconia	30	0.64	41.2	15.6	43.2
	60	0.70	43.3	15.2	41.5
Glass Beads	30	0.64	41.0	14.8	44.2
	60	0.70	45.1	14.6	40.3

2.4.4 Effect of Bed Size and Particle Density

In Table 2.7, percentages of air flow amount through spout, interface, and annulus regions in the small- and large-scale spouted beds having conical angles of 60° and 66°, respectively for zirconia and glass beads particles are given.

Table 2.8 Percentages of air flow amounts through spout, interface, and annulus regions

Particle	γ (°)	D_c (mm)	ρ_p (kg/m^3)	% air flows through spout	% air flows through interface	% air flows through annulus
Zirconia	60	150	6050	44.7	15.0	40.3
	66	250		28.5	10.3	61.2
Glass Beads	60	150	2460	49.2	12.9	37.9
	66	250		29.7	10.7	59.6

It was found that as the particle density increases, the amount of air flow passing through the annulus increases. In addition, it can also be seen from this table, dispersion of the gas into the annulus is significantly higher in the large-scale unit than the small-scale unit. Although the ratio of the superficial velocity to the minimum spouting velocity is different from each other, the increase in the amount of air flows through the annulus in the large scale unit can be explained with the increase in the residence time of the gas in the bed. The effect of bed size on the radial normalized gas velocity distributions for zirconia and glass beads particles is illustrated in Figure 2.13. The distributions are given on the same z/H_b location. This particular axial height was specifically chosen in the middle of the beds to preserve the measurements from the other existing effects near the bed inlet and exit. Because most of the gas fed to the system flows through spout and interface regions for small scale bed, the normalized gas velocities in the spout region were found to be also higher compared to the large-scale unit. Furthermore, the effect of bed size on the normalized velocities measured in the spout region in different scales is more significant for light particles than heavy particles.

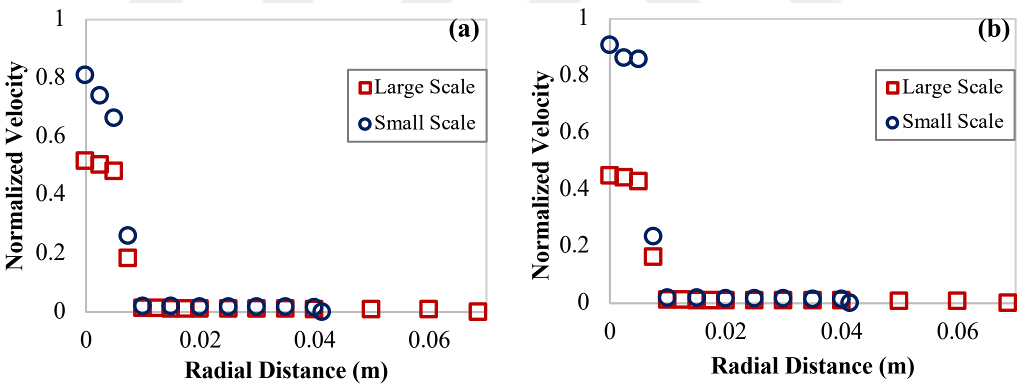

Figure 2.13 Effect of bed size on the radial normalized gas velocity profiles for (a) zirconia, (b) glass beads particles (for large scale unit γ=66°, D_c=250 mm, H_b=144 mm, U_0=1.05U_{ms} ; for small scale unit γ=60°, D_c=150 mm, H_b=100 mm, U_0=1.25U_{ms} ; H_p/H_b=0.5)

2.5 Conclusion

In this chapter, results of Pitot tube measurements are presented for conical spouted beds operated with both low- and high-density particles. It was found that as the axial distance increases from the base of the unit, the interstitial gas velocity decreases for both light and heavy particles and the amount of air going through the annulus section increases. The normalized gas velocities in the spout region increases with increasing cone angle and no significant effect can be seen for the normalized gas velocities in the annulus section. On the other hand, the amount of air that flows through the annulus decreases with increasing cone angle indicating that penetration of the gas from the spout through the annulus becomes harder for spouted beds having wider conical angle. The amount of air flow passing through the annulus increases as the particle density increases. Dispersion of the gas into the annulus region is found higher in the large scale unit compared to the small scale unit mainly because in the large scale spouted bed the spouting gas has more residence time to travel through annulus region.

CHAPTER 3

GAS MIXING IN CONICAL SPOUTED BEDS

3.1 Literature Survey

One of the most favorable characteristics of the conical spouted beds is their unique mixing behavior. Gas mixing experiments are conducted to investigate gas mixing inside the bed. In consequence of gas mixing studies, the gas dispersion coefficient which is a parameter that quantifies the extend of gas mixing is determined.

Two different methods have been used in gas mixing experiments: steady state and unsteady state experiments. In steady state experiments, the tracer gas is supplied to the system continuously. Depending on the measurement point, this kind of experiments could enlighten the radial gas distribution in the bed, flow pattern and radial gas mixing characteristics of the bed and back mixing. The investigation of the radial gas mixing characteristics in the conical spouted beds with steady state tracer gas technique in the literature is very limited and the only study with heavy particles was presented by Çangal (2011) previously in our research group. In this study, due to the difficulties in measurements of the local gas velocities in the annulus region as addressed in this thesis, the radial dispersion coefficients were calculated only for spout region and the effect of particle diameter, gas velocity at the inlet of the bed, conical angle, height of the measurement points on the radial dispersion were investigated. It was reported that these parameters had no significant effect on the radial dispersion coefficients obtained in the spout region of the conical spouted beds.

In contrary to steady state experiments, unsteady state experiments are generally used for quantification of the axial gas mixing and are generally conducted with two types of tracer experiments which are inputs of a pulse or a step function. Step function experiment is applicable as negative step or positive step. The expected inlet and exit concentrations of the real systems for pulse and step functions are illustrated in Figure 3.1 (a) and (b), respectively.

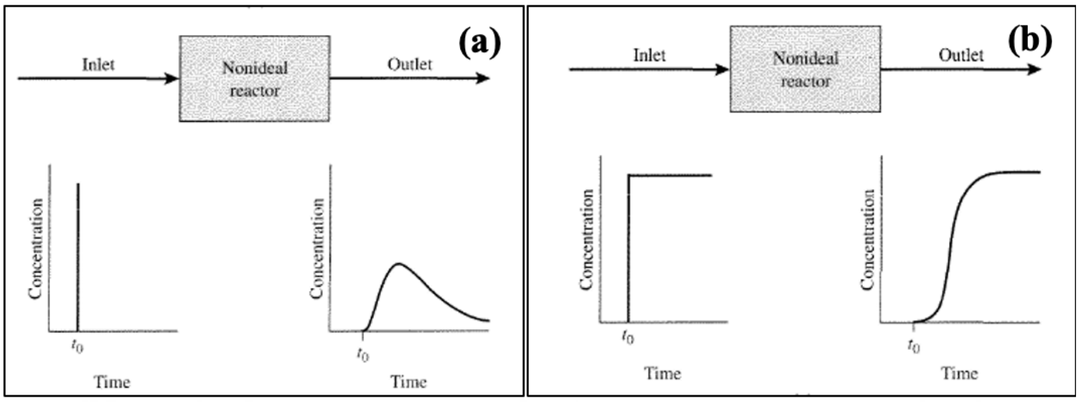

Figure 3.1 Tracer concentrations in real reactors by using (a) pulse, (b) step functions (Davis and Davis, 2003)

The residence time distribution (RTD) curves are obtained by conducting unsteady state tracer gas experiments. The RTD curves are used for recognition of flow pattern in the reactors and determination of the dead zones that can be crucial for predicting the conversion in the reactors (Davis and Davis, 2003). The unsteady state gas mixing studies conducted in spouted beds are summarized in Table 3.1. As can be seen, there is very limited number of gas mixing studies and in all of these studies light particles are used.

Table 3.1 Summary of gas mixing studies

AUTHORS	PARTICLE PROPERTIES			BED PROPERTIES				EXPERIMENT	
	Type	d_p (mm)	ρ_p (kg/m^3)	γ	D_c (mm)	H_c (mm)	H_b (mm)	Tracer	Method
Lim & Mathur (1974)	Wheat Polystyrene	3.45 2.67	1177 1020	60	152	-	457 305 152	Helium	Negative Step Function
Lim & Mathur (1976)	Polystyrene Polystyrene Wheat Millet Glass beads Glass beads Ammonium nitrate Ammonium nitrate	2.93 1.61 3.50 2.15 2.93 1.10 1.99 1.45	1050 1050 1240 1180 2940 2960 1750 1740	60	152 241 292	-	-	Helium	Negative Step Function
Olazar et al. (1995)	Expanded polystyrene	3.5	14	45	50	360	280	Hydrogen	Negative Step Function

Table 3.2 Summary of gas mixing studies in the literature (Continued)

AUTHORS	PARTICLE PROPERTIES			BED PROPERTIES				EXPERIMENT	
	Type	d_p (mm)	ρ_p (kg/m^3)	γ	D_c (mm)	H_c (mm)	H_b (mm)	Tracer	Method
San Jose et al. (1995)	Glass spheres Extruded polystyrene Rice	1-2-3-4-6-8 4.1 3.8	2240 960 1250	45 39 36 33 28	360	360 400 450 500 600	100-340	Hydrogen	Negative Step Function
Wang (2006)	Glass beads	1.16 2.40	2487 2485	45	450	500	396	Helium	Negative Step Function

Lim and Mathur (1974) conducted experiments in a conical-cylindrical spouted bed having conical angle of 60° by using wheat and polystyrene particles (ρ_{wheat}=1177 kg/m^3, $\rho_{polystyrene}$=1020 kg/m^3) for various stagnant bed heights. They applied negative step instead of pulse injection to avoid the disturbance and possible collapse of spout caused by pulse injection. NO_2 gas was used as a tracer in a half bed to observe the gas flow path in the bed visually. The tracer concentration at the inlet gas as stimulus and the tracer concentration at the exit gas at two different locations which are the column axis and middle of the annulus as response were measured. A two-region model allowing the gas flow through spout to annulus was developed to obtain dispersion coefficient. Axially dispersed plug flow in annulus and plug flow in spout was assumed in their model. Mass conservation of the tracer was applied for both regions considering the cross-flow. The axial dispersion coefficient was calculated based on the measurements taken from the annulus. They reported that the calculated axial dispersion coefficients of spouted beds are similar with the axial dispersion coefficients presented for fluidized beds, but are much higher than the ones for packed beds reported in the literature and concluded that axial dispersion coefficient increases with increasing gas velocity in the annulus. They expanded their investigation in their following study (1976) by using various types of particles and updating the gas flow in annulus in their model. They divided the annulus region of their system into curved streamlines instead of using vertically upward flow which was used in their previous model. It was found that dispersion coefficient increased with increasing particle size and bed depth while it showed no significant change with column diameter and orifice diameter. They compared their results with the results of the experiments conducted in similar conditions and particles for packed beds and fluidized beds reported in the literature. The comparison showed that the axial dispersion coefficients of spouted beds are approximately an order of magnitude smaller than those in fluidized beds and higher than those in packed beds.

A new model based on the model of Lim and Mathur (1976) was developed by San Jose et al. (1995) almost a decade later. The model applies the conservation equation of tracer for the spout and the annulus as a two different differentiated flow zones.

San Jose and co-workers conducted their first study (1995) in a spouted bed having a conical angle of 45° with expanded polystyrene particles ($\rho_{polystyrene}$ =14 kg/m^3) and they continued their investigation (1995) by using spouted beds having different cone angles (45°, 39°, 36°, 33°, 28°) with glass beads, extruded polystyrene and rice particles (ρ_{glass}=2420, $\rho_{polystyrene}$ =960, ρ_{rice} =1250 kg/m^3). Hydrogen gas was used as tracer. Inlet and exit concentrations of the tracer were measured. The predicted axial dispersion coefficients and their corresponding tracer concentration as a function of time were calculated by applying the same gas mixing model in both of their studies. When the obtained dispersion coefficients were compared with the ones found in the literature, it was seen that the calculated dispersion coefficients of the conical spouted beds were between coefficients of fixed beds and fluidized beds and in the same order of magnitude with coefficients of cylindrical spouted beds. Considering different geometrical properties of the spouted beds used in the experiments, they proposed the only correlation (1995) available in the literature for calculation of the gas dispersion coefficient in conical spouted beds as follows:

$$D = 6.3 \times 10^{-7} \left(\frac{D_b}{D_0}\right)^{3.72} \left(\frac{D_0}{D_i}\right)^{-2.1} Ar^{0.46} \times \left(\tan\frac{\gamma}{2}\right)^{0.84} \left(\frac{U}{U_{ms}}\right)^{-1.1} \tag{3.1}$$

$$D_b = 2H_0 \tan\left(\frac{\gamma}{2}\right) + D_0 \tag{3.2}$$

where H_b is the stagnant bed height, D_b is the upper diameter of the stagnant bed height, D_0 and D_i is the diameter of the contactor base and of the inlet, and Ar is the Archimedes number.

Lastly, Wang (2006) defined the Peclet number for a conical spouted bed with Eq. 3.3 where L is accepted as streamtube length, U_i is the interstitial gas velocity and D is the dispersion coefficient.

$$Pe = \frac{L\,U_i}{D} \tag{3.3}$$

Because the gas velocity has a radial distribution in the system and streamtube length changes depending on the radial position, Wang (2006) presented radial distribution of the Peclet number in his system. According to simulation results, the dispersion coefficient which gives the better agreement with experiments has an order of 10^{-4}. He also calculated experimental Peclet numbers by using the variance with related equation (Levenspiel, 1979). He compared the residence time distributions and Peclet numbers obtained from the experiments with the ones obtained from the CFD software ANSYS FLUENT which was used for simulating the same conditions of the spouted bed used in the experiments. Furthermore, the difference between the radial distribution of the experimental mean residence time and simulated one was tried to be eliminated modifying the axial superficial gas velocities. Although, the gas velocities were modified, the experimental Peclet numbers could be not verified with CFD results. The difference between the radial distribution of the experimental and simulated Peclet numbers could not be eliminated even by using all possible values of the dispersion coefficient investigated.

As can be inferred from the literature review, the available gas mixing studies in the literature conducted in spouted beds are limited and were mainly conducted in spouted beds operating with light particles. Therefore, the objectives of this part of the study were to develop a system that can carry out unsteady experiments measuring the transient tracer concentrations and investigate the gas axial mixing behavior in conical spouted beds operating with both low and high density particles.

3.2 Measurement System for Gas Mixing Studies

For the investigation of the gas mixing behavior in spouted beds operating with low and high density particles, a gas concentration measurement system is designed and manufactured in this study. The system includes infrared gas analyzer, automatic injection system, control station and an adjustable sampling system suitable for different dynamic conditions. A photograph of the measurement system is given in Figure 3.2.

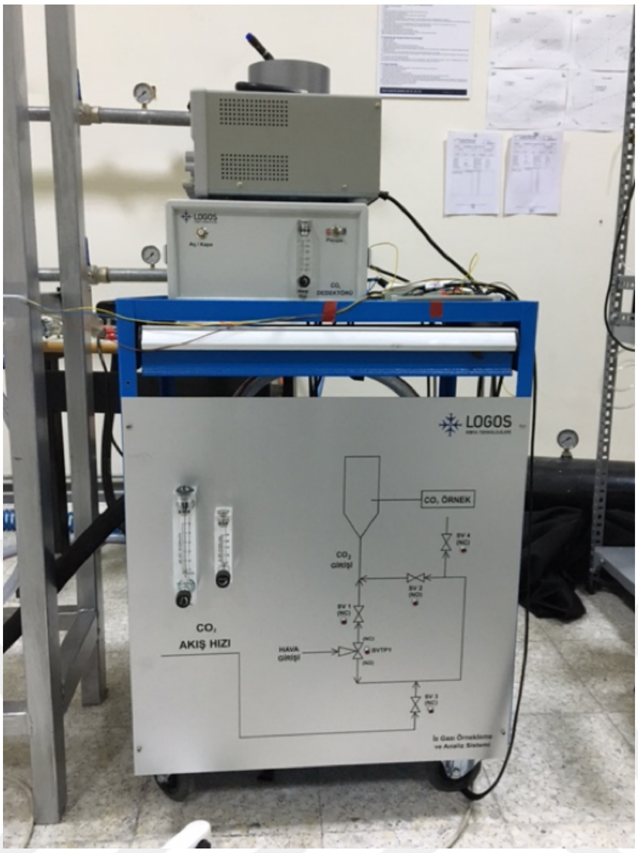

Figure 3.2 Photograph of the gas concentration measurement system

The system is able to carry out both steady and unsteady tracer experiments. For the unsteady tracer experiments, the working principle of the system is based on the injection of a tracer gas to the reactor as pulse, positive step or negative step injection and monitoring and recording the time dependent tracer gas concentration with an infrared gas analyzer. Carbon dioxide is used as the non-reactive tracer gas. Flow and instrumentation diagram of the developed system is shown in Figure 3.3.

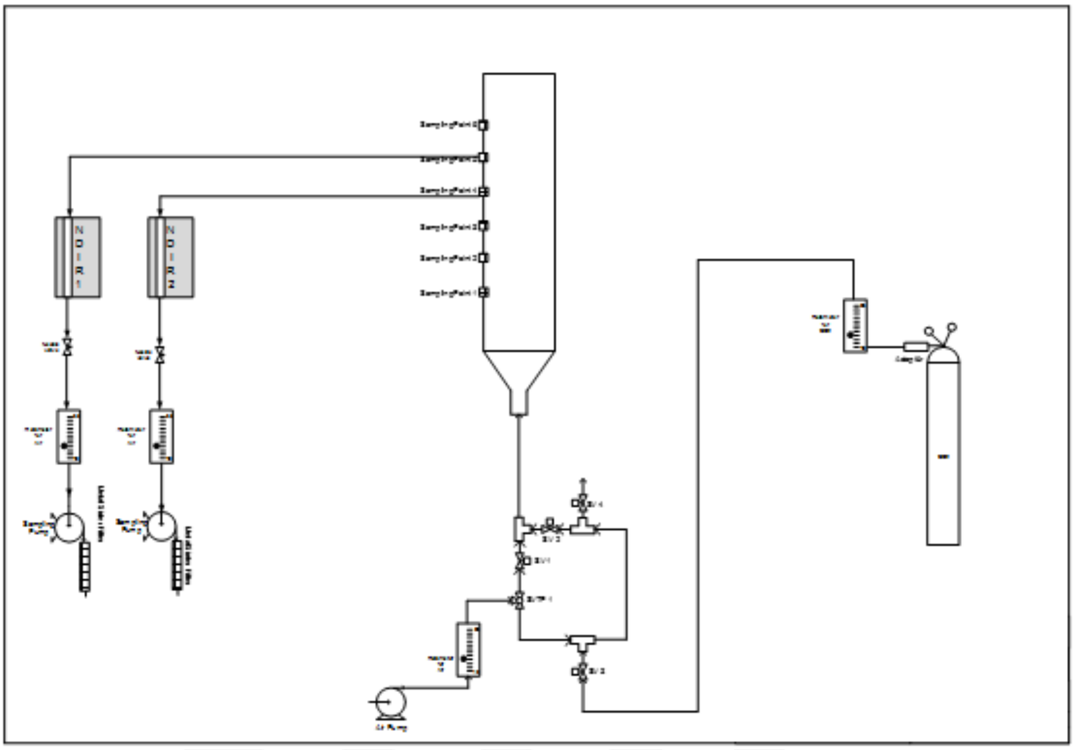

Figure 3.3 Instrumentation diagram of the measurement system

The system consists of two sampling line that can operate independently from each other and one supply line. There are two NDIR CO_2 sensors, rotameters to adjust the flow of CO_2 and vacuum pumps to suck the sample in the sampling line. The NDIR CO_2 sensors operate in the range of %0-10 volume and the output of the sensors is analog signal of 0-1 volt depending on the concentration value. The supply line consists of an air compressor, CO_2 tank, CO_2 and air flowmeters and solenoid valves that can operate in positive step, negative step or pulse modes. In this study, the tracer is injected as negative step function.

The suction velocity of the system is adjustable between 100 cm^3/min and 1000 cm^3/min. To achieve an isokinetic sampling and not to disturb the flow in the beds, a sampling probe having an outer diameter of 5 mm and an inner diameter of 3.9 mm is connected to vacuum pump and the suction velocity is determined as 200 cm^3/min. In that way, velocity at the tip of probe is fixed as 0.28 m/s which is a lower value than the velocities measured in the annulus section of the spouted beds for every operating condition.

To convert NDIR analog signal to digital signal and to control the solenoid valves, the whole system is operated and controlled by LabVIEW software. All solenoid valves are defined to the software considering the electrical structure of the measurement system to provide the step tracer experiment mode or pulse experiment mode. With the written code all solenoid valves can be controlled by individually as well as the valves can be adjusted for negative step experiments with only one command given by the LabVIEW. In addition, the elapsed time between the valves can be measured by the code and reported as an output. The written code for concentration measurements is given in Appendix C.

Considering the measuring range of the sensor is % 0-10 volume and 0-1 Volt analog signal is produced depending on the tracer concentration as output, the relation between the concentration and the analog signal is assumed to be linear and Eq. 3.4 is used for conversion.

$$Concentration = 10 * (Voltage) \tag{3.4}$$

The calibration of the system was done by using pure nitrogen gas for ZERO and %9 CO_2 balanced with nitrogen gas for SPAN. The sampling frequency was set as 100 Hz. Two sensors were used to take measurements from two different locations simultaneously and various problems were encountered and solved during the course of measurements. Generally, conducting transient experiments is a very challenging task especially when the time between the input (injection) and output (sampling) is very short (in the order of 100 ms in the annulus) as in this work. Therefore, fast response sensors were used and dead volumes between the sampling probe and the sensors were minimized.

3.3 Gas Mixing Model for Conical Spouted Beds

To quantify the gas mixing characteristic of the conical spouted beds by means of the dispersion coefficient, a gas mixing model is developed based on the model of San Jose et al. (1995) for conical spouted beds. The model requires the knowledge of the local gas velocity distribution in the conical spouted bed for both spout and annulus region. The main assumptions of the model are:

- The gas travels through the spout in plug flow.
- There is gas transfer through the interface from the spout to the annular zone.
- There is no gas transfer between the streamtubes.
- In each streamtube, both convection and dispersion occur.
- Dispersion coefficient, D, is same for all streamtubes.

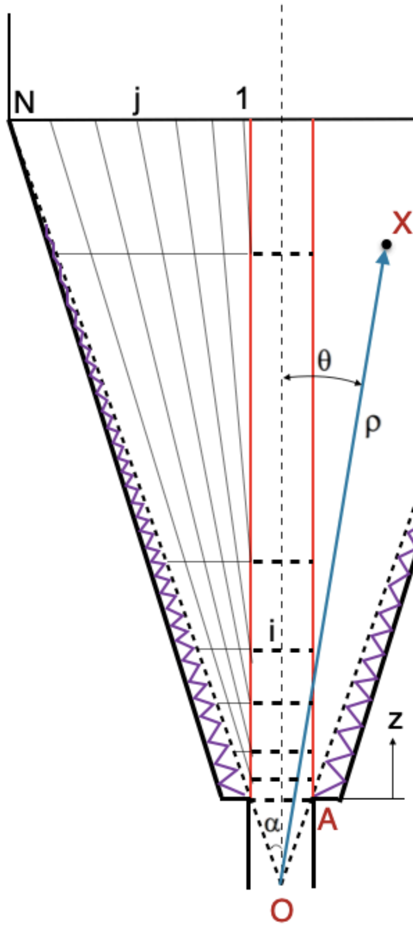

Figure 3.4 Gas mixing model

According to the model, the system consists of two main parts: spout and annulus as shown in Figure 3.4. The spout is divided into several axial control volumes which is shown with an index i. The annulus, in addition to axial compartments, is divided into N number of equiangular streamtubes. The intersection point of the dashed lines traced from top of the side wall (B) to inside corner of bed inlet (A) is accepted as origin point (O). The narrow areas between these lines and the bed walls are directly related with the contactor geometry and these areas are assumed to be dead zones shown with purple lines in Figure 3.4. Any random point (X) in the gas flow is represented by the longitudinal (ρ) and spherical (θ) coordinates, respectively.

In negative step experiment, first, the system is operated with the tracer injection until the system reaches to steady state. Then, the valve of the tracer gas injection is closed and this time is recorded as the start of the negative step (t=0). For annulus region, the conservation equation of tracer mass is applied considering both convection and dispersion in the streamtube direction neglecting convective and diffusive transport between the streamtubes. The governing transport equation and corresponding initial and boundary conditions for negative step tracer gas experiments in annulus region are given below:

$$\frac{\partial C_A}{\partial t} = -U_{ij}\frac{\partial C_A}{\partial \rho} + D\frac{\partial^2 C_A}{\partial \rho^2} \tag{3.5}$$

where the first term on the left-hand side is the time rate of change of the tracer gas and the first and second terms on the right-hand side represent the convective and diffusive transport in the streamtube direction, respectively.

For $t \leq 0$,

I.C. $C_A = 1$ $\longrightarrow$ for negative step tracer experiment (3.6)

For $t > 0$,

B.C. 1 $D\frac{\partial C_A}{\partial \rho} = (C_A - C_S)(U_{ij})$ $\longrightarrow$ at the inlet of streamtube (3.7)

B.C. 2 $\frac{\partial C_A}{\partial \rho} = 0$ $\longrightarrow$ at the outlet of streamtube (3.8)

Solution of the annulus region requires the tracer concentration in the spout region as a function of time and position as a boundary condition at the interface. The flow is assumed to be plug flow in the spout region. There is mass transfer through interface from the spout to the annulus region. The governing transport equation and corresponding initial and boundary conditions for negative step tracer gas experiments in spout region are given below:

$$\frac{\partial C_S}{\partial t} + \overline{U_S}\frac{\partial C_S}{\partial z} = 0 \tag{3.9}$$

where $\overline{U_s}$ is the interstitial gas velocity in the spout.

For $t \leq 0$,

I.C. $\quad C_S = 1 \quad$ (3.10)

For $t > 0$,

B.C. $\quad z = 0 \quad C_S = 0 \quad$ (3.11)

At the beginning of the negative step (t=0), the concentration at each position in the spout is taken to be equal to the steady state concentration (C_s). The tracer concentration becomes zero at the spout entrance (z=0) when t>0. All the governing differential equations together with their corresponding initial and boundary conditions are solved together by using the MATLAB code developed in this study.

3.4 Data Processing and Solution of the Model

3.4.1 Determination of the measurement points

The gas mixing experiments were conducted in two small scale spouted beds having conical angle of 30° and 60°. The measurement points were determined based on the gas mixing model. As stated before, the narrow areas just near the bed wall were accepted as dead zones. The existence of these dead zones changed the angle of the experimental region. The new imaginary cone angle was calculated by using the equation given below.

$$\alpha = \tan^{-1}\left[\frac{r_B - r_S}{H_b}\right] \tag{3.12}$$

The annulus section of the system was divided into N = 4 equiangular streamtubes. During the gas velocity measurements, it was shown that gas velocity profile was symmetrical around the center of the conical spouted bed. With this knowledge, in gas mixing experiments, the measurements were taken from the half of the bed. In this study, tracer concentrations were measured at the inlet of the spouted bed and at the middle point of the exit of each streamtubes. Middle points of the inlet and the exit of every control volume were numbered as nodes. For the determination of the exact locations of the nodes, the geometrical structures of the systems were drawn by using the AutoCAD software. These drawings are given in Appendix D. The node numbering of the system is shown in Figure 3.5. The measurements were taken from Nodes 0, 5, 9, 12, 13 and 14.

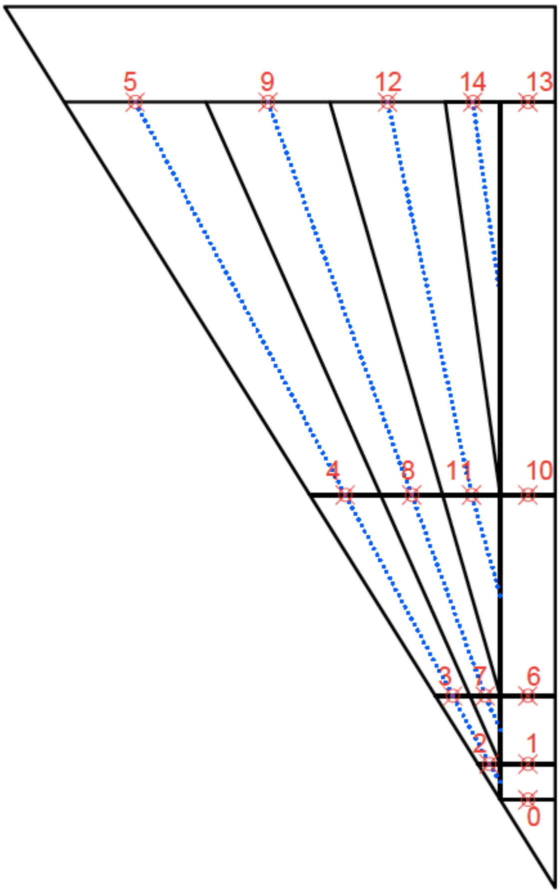

Figure 3.5 Node numbering

3.4.2 Smoothing of the experimental data

During the transient measurement of the tracer gas concentrations at the inlet and exit in negative step experiments, the combined effects of slight fluctuations in air flowrate, pressure waves caused by the closure of the injection valve and solids motion in the bed and possible measurement noise result in some random variation (error) of the discreet data around a local mean value. In order to minimize the effects of this uncertainty on the determination of the start time (t = 0) and dispersion coefficient and increase the level of repeatability in consecutive measurements, the transient discreet data was smoothened using a data filtering software, JMP.

With the help of this software, a smoothing spline was fitted to each experimental data set. A set of third degree polynomials was attached by the cubic spline method and a continuous and smooth curve was obtained. This method estimates $\hat{f}$ by using the combination of the sum of squared errors of observed pairs (x_i, y_i) and a penalty for curvature integrated over the curve extent as a function that should be minimized. Cubic smoothing spline is defined as (Hastie and Tibshirani, 1999):

$$\hat{f} = argmin_f \sum_{i=1}^{n} (y_i - f(x_i))^2 + \lambda \int_a^b (f''(x))^2 dx \quad (3.13)$$

The lambda (λ) is an adjustable parameter which effects the weight of the error term in the objective function. When the lambda approaches to zero; results become more flexible and curved fit. When the lambda approaches to infinity, the resulting curve converges a straight line. In this study, the lambda was determined as 0.01 for all of the experimental data and illustrations of fitted curves of the measurements taken from the center of the spout at the inlet and the exit of the same system are given in Figure 3.6.

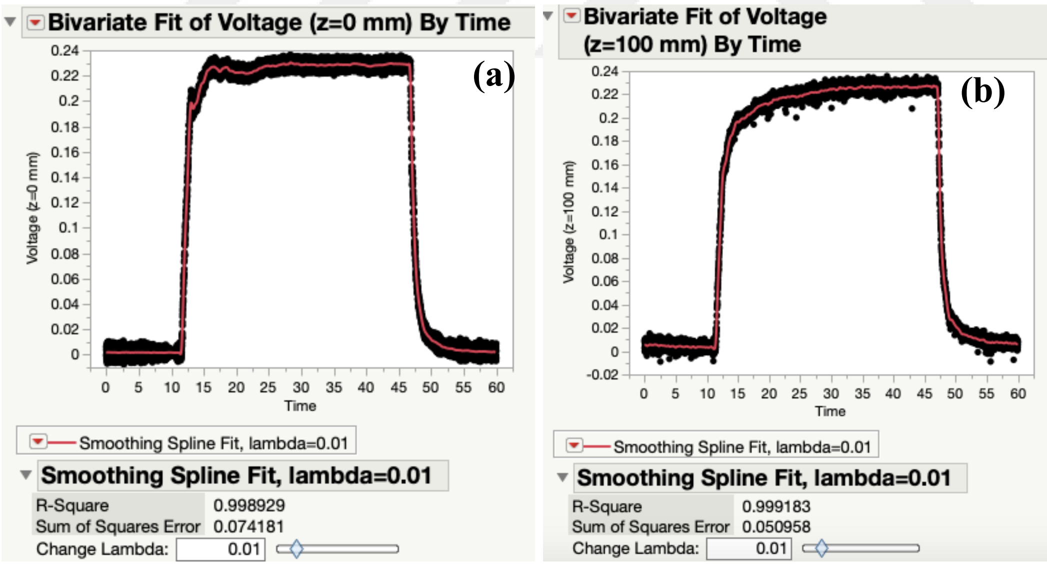

Figure 3.6 Resulting curves over experimental data taken from (a) the inlet (z=0 mm) and (b) the exit (z=100 mm) (ρ_p=2460 kg/m^3, d_p=1 mm, γ=60°, H_b=100 mm, U_0=1.25U_{ms})

After smoothing of all experimental data, the smoothed data is extracted from the software. The measured concentrations of the tracer gas were normalized with steady state concentrations and the point of $t = 0$ is determined.

3.4.3 Determination of the boundary condition at the inlet of the streamtubes

In an experiment, two sampling probes were used simultaneously. One of them was located at the inlet of the bed (Node 0) and the other one was located at the exit of one streamtube. Since there were 4 streamtubes and spout, the experiments were repeated for each which means that 5 experiments were conducted to obtain time dependent tracer concentration change in conical spouted bed. Although the inlet boundary condition given in Eq. 3.11 represents a perfect negative step, the measurements at $z = 0$ showed that step change given at the inlet of the bed was not perfect possibly due to response time of the valves and lag time between the tip of probe and the sensor. Therefore, the measurements (measured time dependent tracer concentration) taken at the Node 0 was defined as boundary condition in the model. In order to obtain the full picture at an operating condition, experiments were repeated for every streamtube and spout while the average of the measured concentration at Node 0 was used in defining the boundary condition.

A comparison of the transient concentration profiles measured at Node 0 under the same operating condition is given in Figure 3.7. As can be seen from this figure, experiments were repeatable and therefore the average of the repeated measurements was used as the inlet boundary condition in the model.

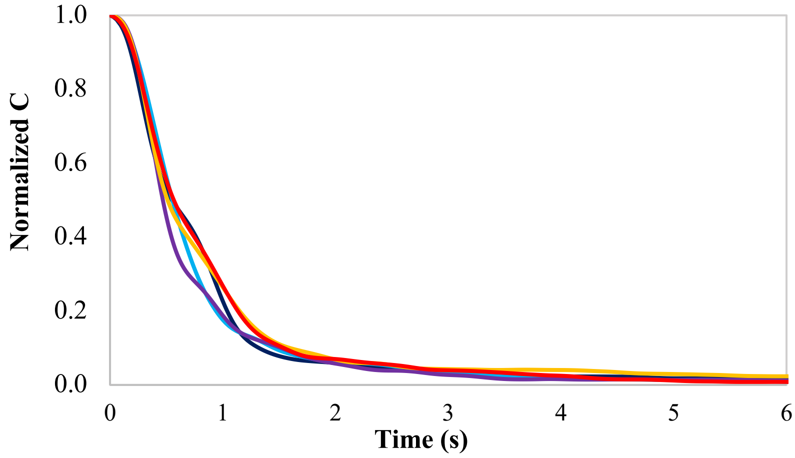

Figure 3.7 Comparison of the measured tracer concentration profiles at the inlet (ρ_p=6050 kg/m^3, d_p=1 mm, γ=30°, H_b=180 mm, z=0 mm, U_0=1.25U_{ms})

3.4.4 Developed Model

In this study, in order to obtain the transient local concentration profiles inside the spouted bed, a model was developed to numerically solve the governing differential equations together with their corresponding initial and the boundary conditions. The model was developed using MATLAB Software. In the model, the partial differential equation (PDE) developed for spout region (Eq. 3.9) was first converted into an ordinary differential equation (ODE) by utilizing 2-point upwind differencing scheme for the spatial derivative $\frac{\partial c_S}{\partial z}$ as follows:

$$\frac{\partial c_{S_i}}{\partial t} = -\overline{U_S}_i \left[\frac{c_{S_i} - c_{S_{i-1}}}{\Delta z}\right] \tag{3.14}$$

where $\overline{U_S}$ is the local interstitial gas velocity in the spout that varies with position. To be able to use $\overline{U_S}$ in the model, the gas velocity profiles measured and presented in Chapter 2 were expressed by exponential functions.

Same procedure was also followed for annulus section where the PDE of the annulus section was converted into an ODE by using 2-point upwind differencing scheme as follows:

$$\frac{\partial C_{A_i}}{\partial t} = -U_{ij}\left[\frac{C_{A_i} - C_{A_{i-1}}}{\Delta\rho}\right] + D\left[\frac{C_{A_{i+1}} - 2C_{A_i} + C_{A_{i-1}}}{\Delta\rho^2}\right] \tag{3.15}$$

The boundary conditions can also be re-written as:

B.C. 1 $$D\left[\frac{C_{A_{i+1}} - C_{A_i}}{\Delta\rho}\right] = (C_{A_i} - C_{S_i})(U_{ij}) \tag{3.16}$$

$$C_{A_i} = \frac{DC_{A_{i+1}} + C_{S_i}U_{ij}\Delta\rho}{U_{ij}\Delta\rho - D} \tag{3.17}$$

B.C. 2 $$\frac{C_{A_{i+1}} - C_{A_i}}{\Delta\rho} = 0 \tag{3.18}$$

where U_{ij} is the interstitial gas velocity at the interface. Because the local gas velocities in the annulus section and the variation of this velocity axially and radially is very small compared to the velocities in the spout region, the average of the local gas velocities in the annulus section was calculated using the results presented in Chapter 2. The average gas velocity in the annulus section is defined as constant U_{ij} in the model.

The number of nodes in the model was selected to be equal to the number of measurement points. for this purpose, the systems were divided into 4 equiangular streamtubes having 4^o in 30^o conical spouted bed and 8^o in 60^o conical spouted bed which resulted in 14 nodes for both of the systems.

These set of ODEs were solved simultaneously by an ODE solver. For this purpose, Ode15s[1] which is an implicit and a variable step, variable order solver which uses numerical differentiation formulas (NDFs) based on backward differentiation formulas (BDFs) was used. BDFs, also known as Gear's method (1971), are introduced for stiff ODEs and then extended to differential algebraic equations (DAEs). Therefore, Ode15s is a suitable solver for the stiff differential equations and differential algebraic equations. NDFs are more accurate and stable than BDFs and

[1] The 15 indicates that the numerical differentiation formulas of orders 1 to 5 and 's' indicates the stiffness.

are the default method for Ode15s (Celaya et al., 2014). The larger steps can be used by NDFs with same accuracy.

Because the sampling frequency of the measurement system was set as 100 Hz, the time step was chosen as 0.01 second and total sampling time was determined to be 8-10 second. In addition, solution of the ODEs requires the information of dispersion coefficient, D. To predict the dispersion coefficient, for each D value in the range of 0-0.1 m^2/s with 10^{-4} increments, the concentration change of the tracer gas was calculated by the ODE solver. The minimum sum of squares between the calculated and measured values of the tracer concentration over the entire time range was used to find the best fit for the dispersion coefficient.

A sample calculation for the application of the whole process explained above is given in the Appendix E.

3.5 Results & Discussion

3.5.1 Repeatability Experiments

Repeatability experiments were conducted in conical spouted bed having 60^o conical angle operating with 3 different particles. Experiments were conducted on different days at the same operating conditions. The exit tracer concentration profiles measured at different radial positions are given in Figures 3.8-3.10 for zirconia, alumina and glass particles, respectively. The results prove that the experiments were repeatable for all experiments conducted using all three types of particles.

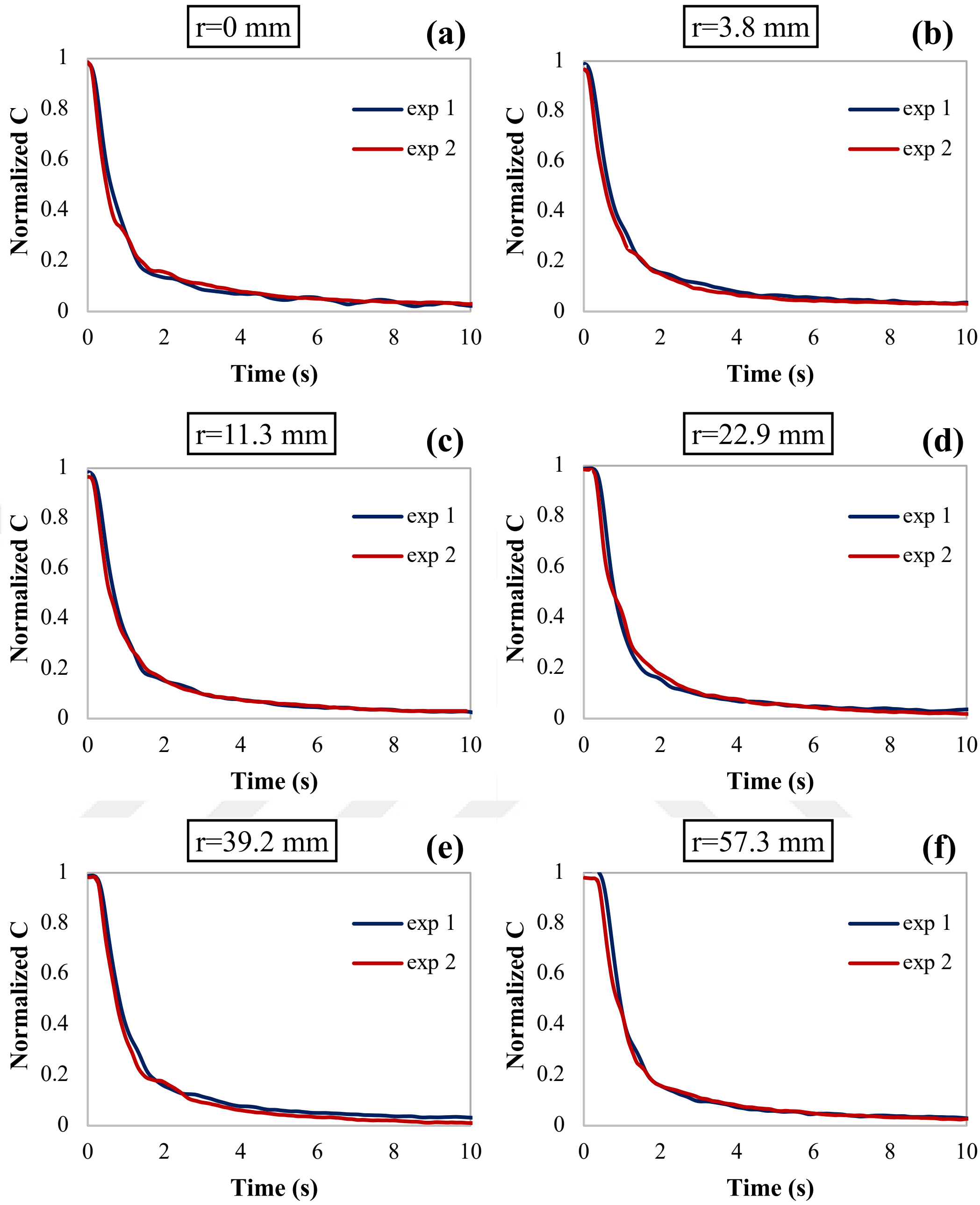

Figure 3.8 Repeatability experiments for of zirconia particles at different radial positions (a) r=0 mm, (b) r=3.8 mm (Node 13), (c) r=11.2 mm (Node 14), (d) r=22.9 mm (Node 12), (e) r=39.2 mm (Node 9), (f) r=57.3 mm (Node 5) (ρ_p=6050 kg/m^3, d_p=1 mm, γ=60°, H_b=100 mm, U_0=1.25U_{ms})

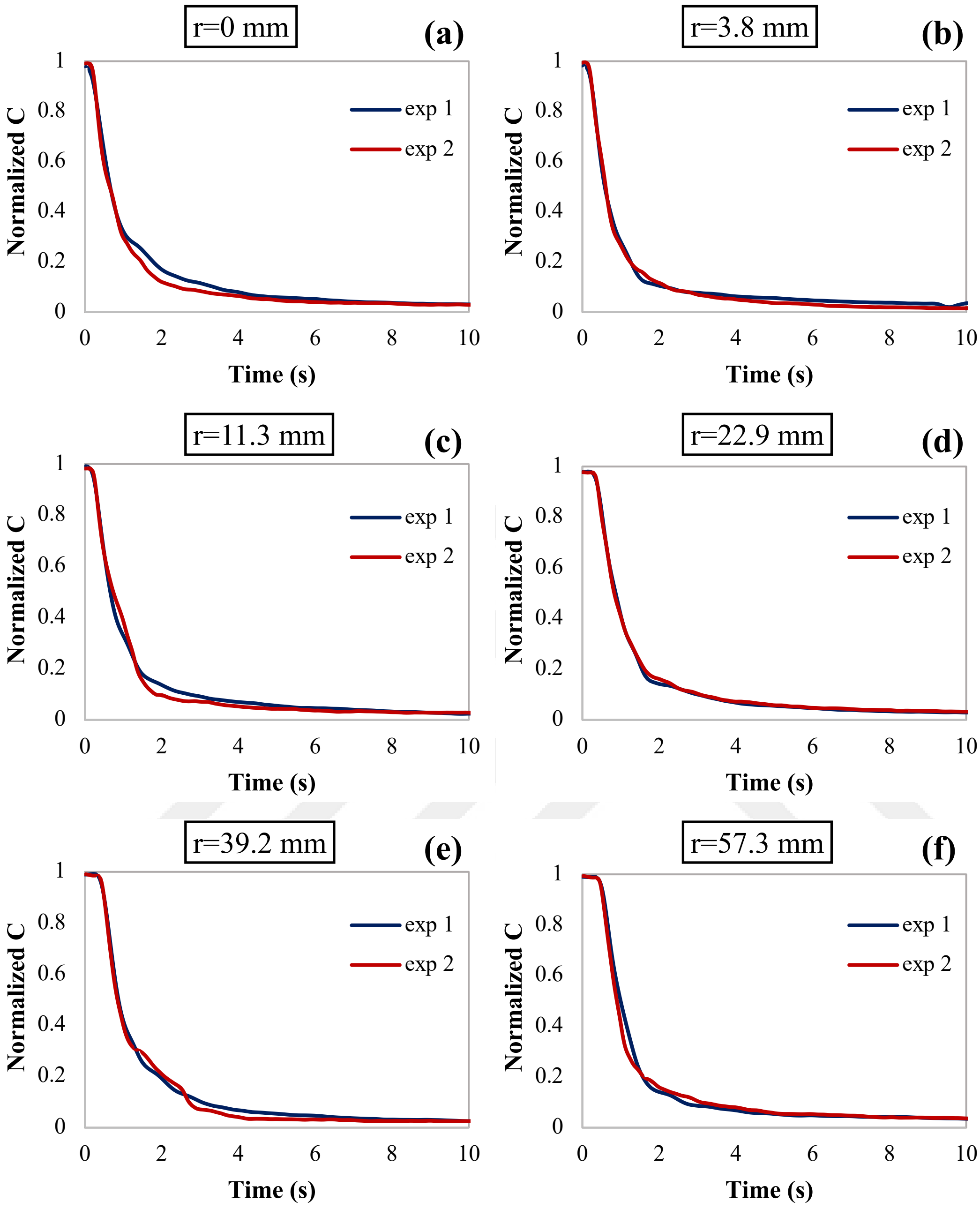

Figure 3.9 Repeatability experiments for of alumina particles at different radial positions (a) r=0 mm, (b) r=3.8 mm (Node 13), (c) r=11.2 mm (Node 14), (d) r=22.9 mm (Node 12), (e) r=39.2 mm (Node 9), (f) r=57.3 mm (Node 5) (ρ_p=3700 kg/m^3, d_p=1 mm, γ=60°, H_b=100 mm, U_0=1.25U_{ms})

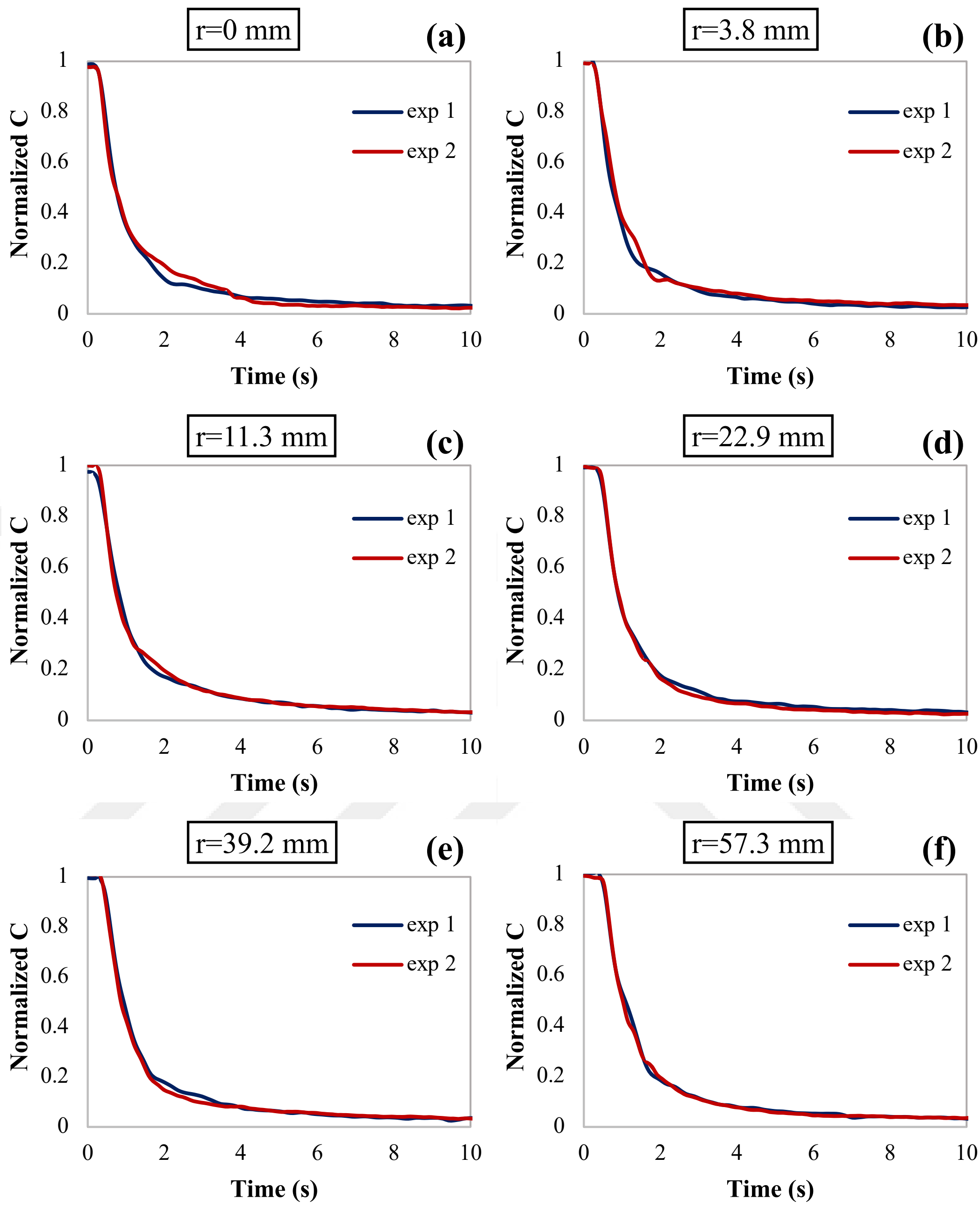

Figure 3.10 Repeatability experiments for of glass beads particles at different radial positions (a) r=0 mm, (b) r=3.8 mm (Node 13), (c) r=11.2 mm (Node 14), (d) r=22.9 mm (Node 12), (e) r=39.2 mm (Node 9), (f) r=57.3 mm (Node 5) (ρ_p=2460 kg/m^3, d_p=1 mm, γ=60°, H_b=100 mm, U_0=1.25U_{ms})

3.5.2 Gas Mixing Experiments

The axial gas mixing experiments were conducted in conical spouted beds operating with 3 different types of particles and operating conditions of the experiments given in table below.

Table 3.3 Operating conditions of the gas mixing experiments

	Particle	ρ_p (kg/m^3)	H_b (mm)	U_0/U_{ms}	U_{ms} (m/s)
60°	Zirconia	6050	100	1.25	35.4
	Alumina	3700	100	1.25	30.2
	Glass Beads	2460	100	1.25	24.1
30°	Zirconia	6050	180	1.25	44.3
	Glass Beads	2460	180	1.25	25.0

The measured concentration profiles are compared with the ones predicted by the gas mixing model and the dispersion coefficient which provides the closest match between the measured and the predicted profiles is determined. The measured and predicted local transient concentration profiles are compared in Figures 3.11-3.15 for all cases investigated in this study. The graphs are presented in terms of radial positions of nodes from the center of the spout (a) to the bed wall (e) and the experimental radial profiles of the tracer are given in (f) section.

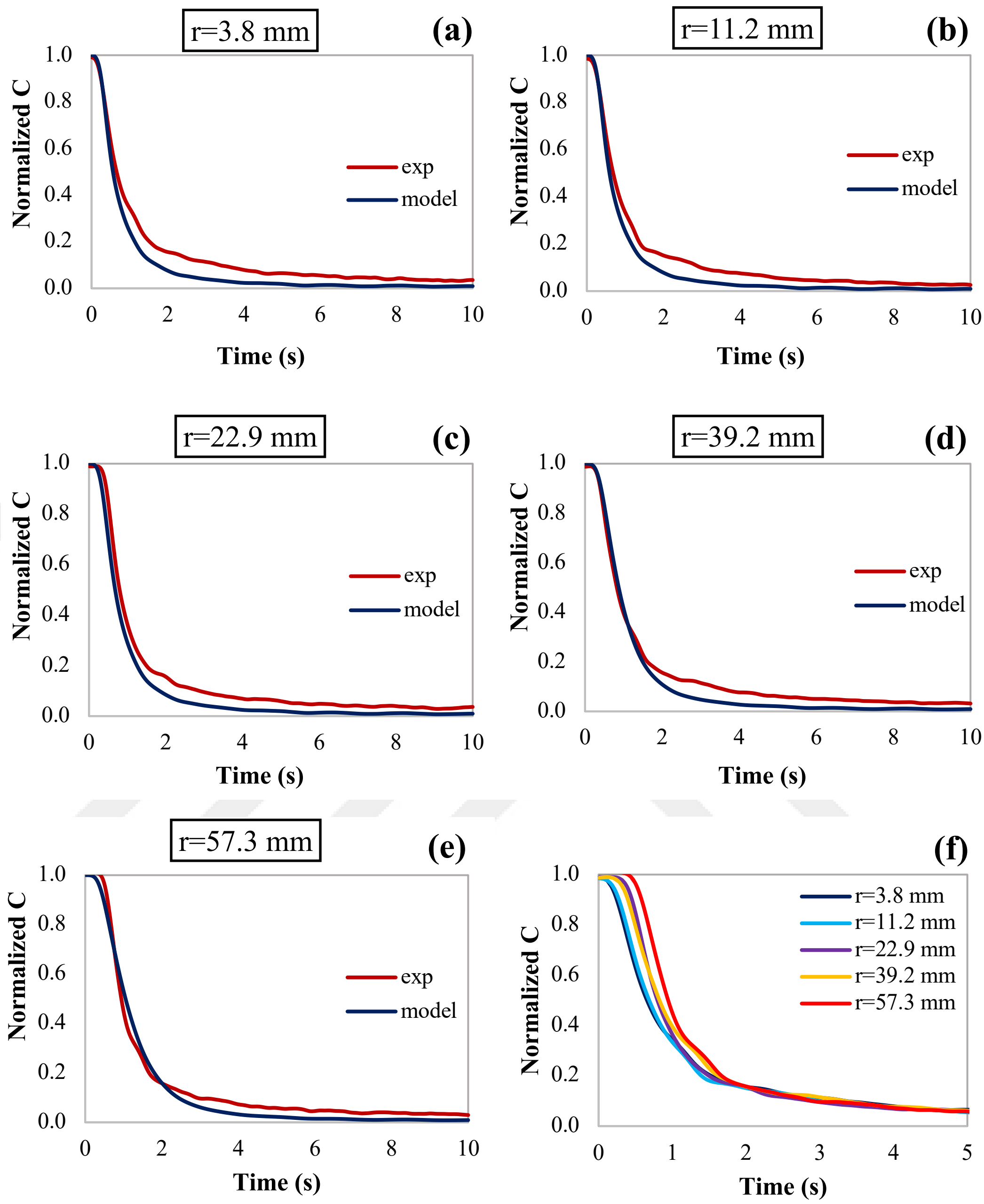

Figure 3.11 Comparison of experimental and predicted tracer concentration profiles at different radial positions (a) r=3.8 mm (Node 13), (b) r=11.2 mm (Node 14), (c) r=22.9 mm (Node 12), (d) r=39.2 mm (Node 9), (e) r=57.3 mm (Node 5), (f) experimental tracer profiles (ρ_p=6050 kg/m^3, d_p=1 mm, γ=60°, H_b=100 mm, U_0=1.25U_{ms}, D=0.0608 m^2/s)

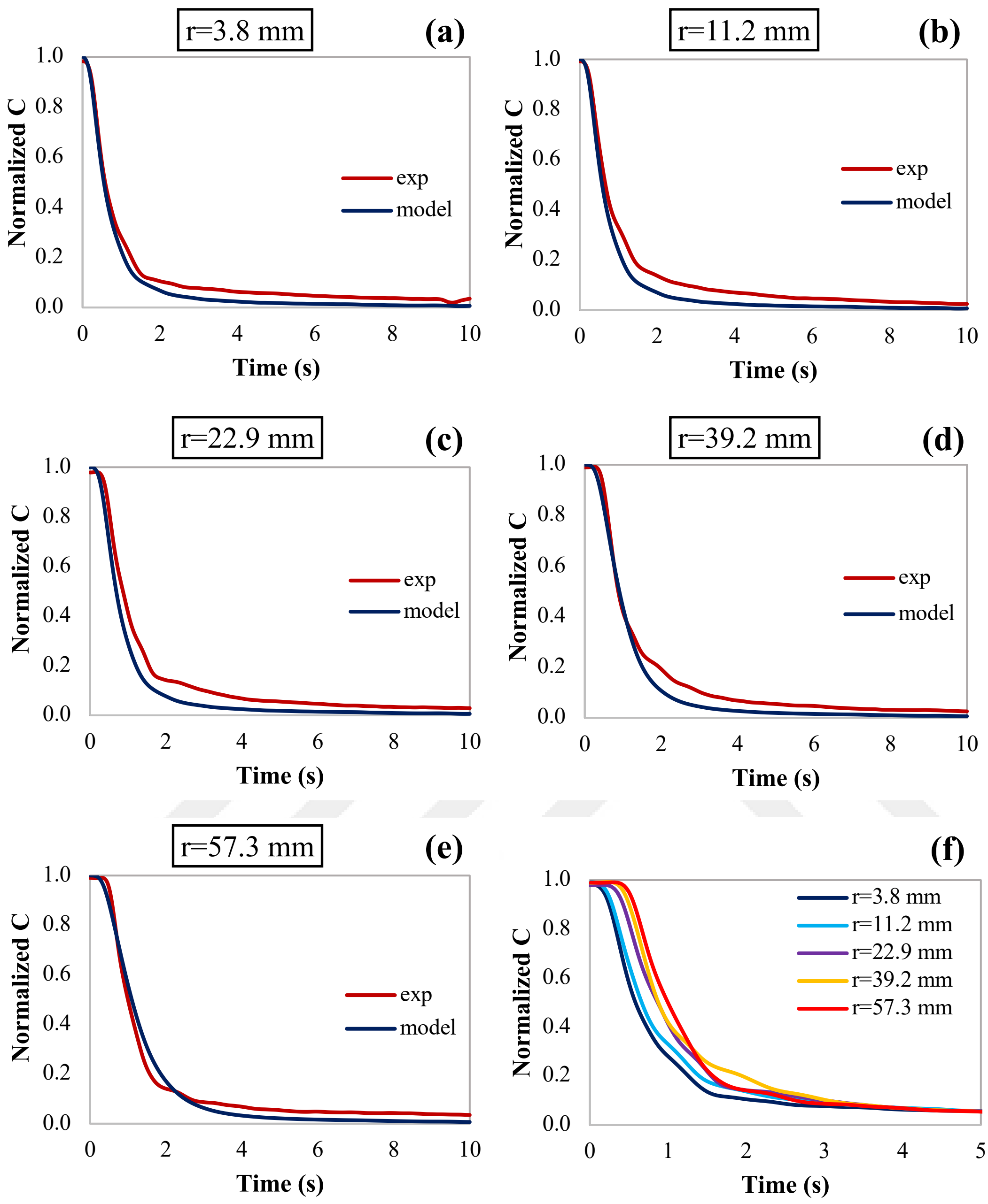

Figure 3.12 Comparison of experimental and predicted tracer concentration profiles at different radial positions (a) r=3.8 mm (Node 13), (b) r=11.2 mm (Node 14), (c) r=22.9 mm (Node 12), (d) r=39.2 mm (Node 9), (e) r=57.3 mm (Node 5), (f) experimental tracer profiles (ρ_p=3700 kg/m^3, d_p=1 mm, γ=60°, H_b=100 mm, U_0=1.25U_{ms}, D=0.0469 m^2/s)

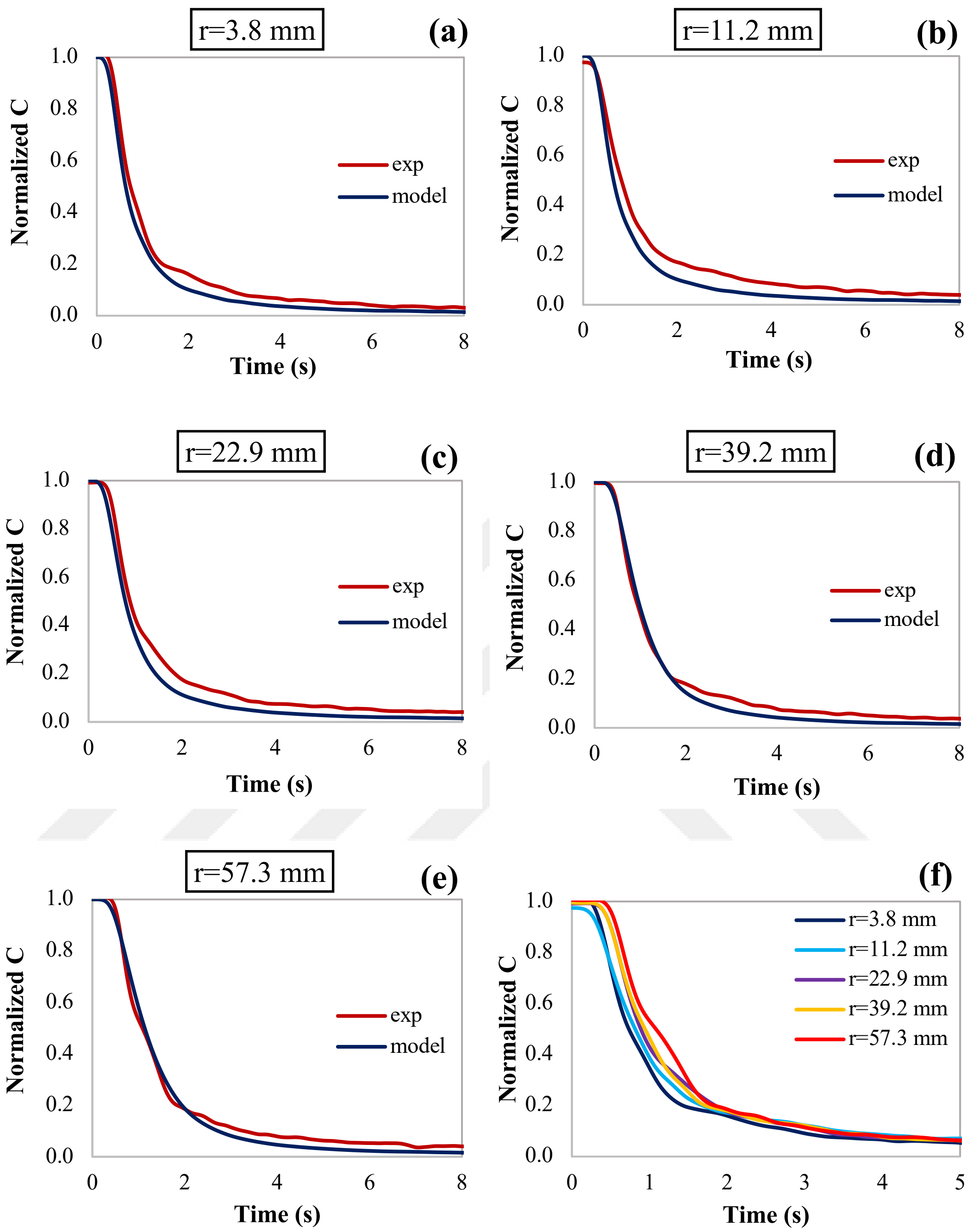

Figure 3.13 Comparison of experimental and predicted tracer concentration profiles at different radial positions (a) r=3.8 mm (Node 13), (b) r=11.2 mm (Node 14), (c) r=22.9 mm (Node 12), (d) r=39.2 mm (Node 9), (e) r=57.3 mm (Node 5), (f) experimental tracer profiles (ρ_p=2460 kg/m^3, d_p=1 mm, γ=60°, H_b=100 mm, U_0=1.25U_{ms}, D=0.0175 m^2/s)

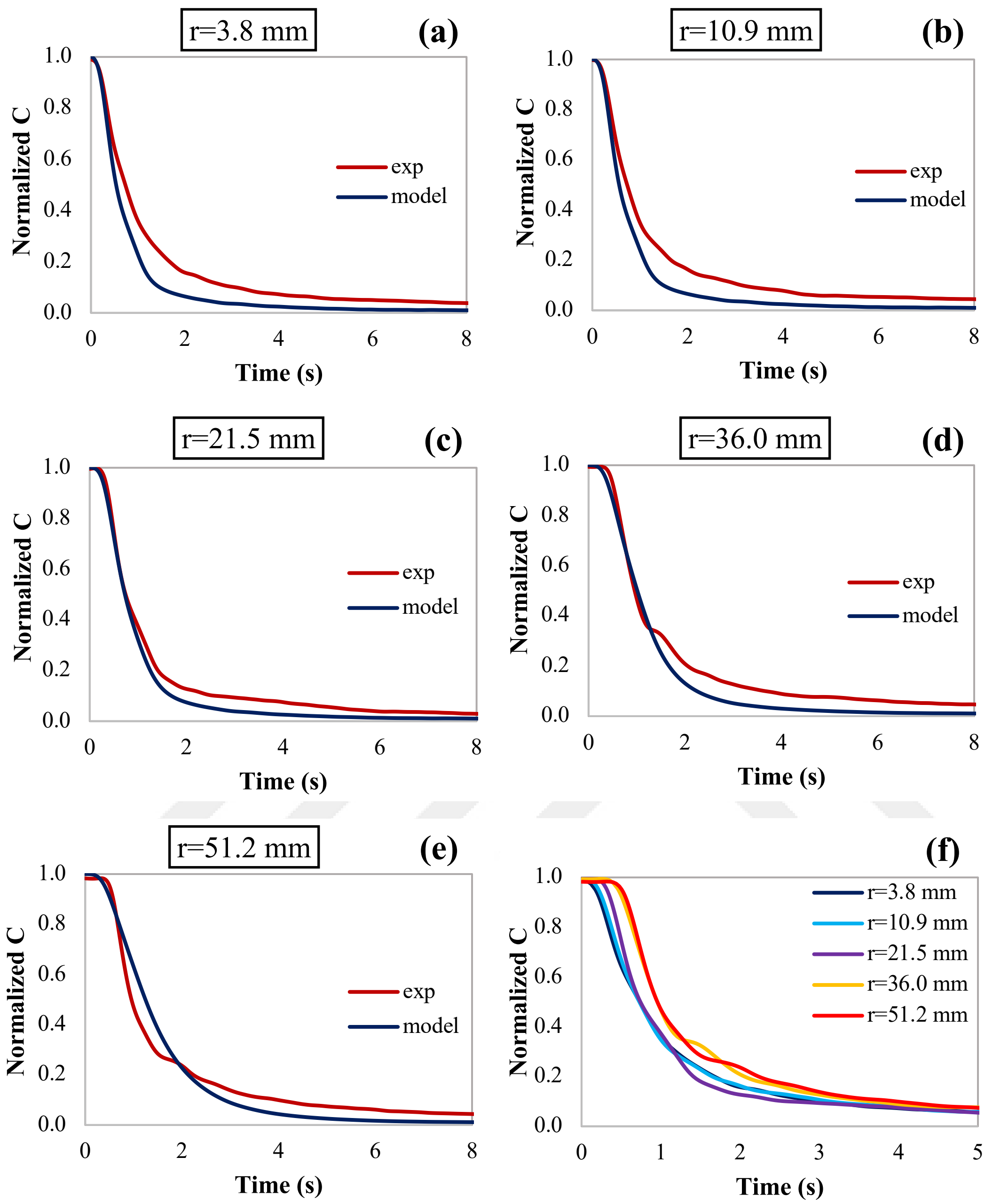

Figure 3.14 Comparison of experimental and predicted tracer concentration profiles at different radial positions (a) r=3.8 mm (Node 13), (b) r=10.9 mm (Node 14), (c) r=21.5 mm (Node 12), (d) r=36.0 mm (Node 9), (e) r=51.2 mm (Node 5), (f) experimental tracer profiles (ρ_p=6050 kg/m^3, d_p=1 mm, γ=30°, H_b=180 mm, U_0=1.25U_{ms}, D=0.0935 m^2/s)

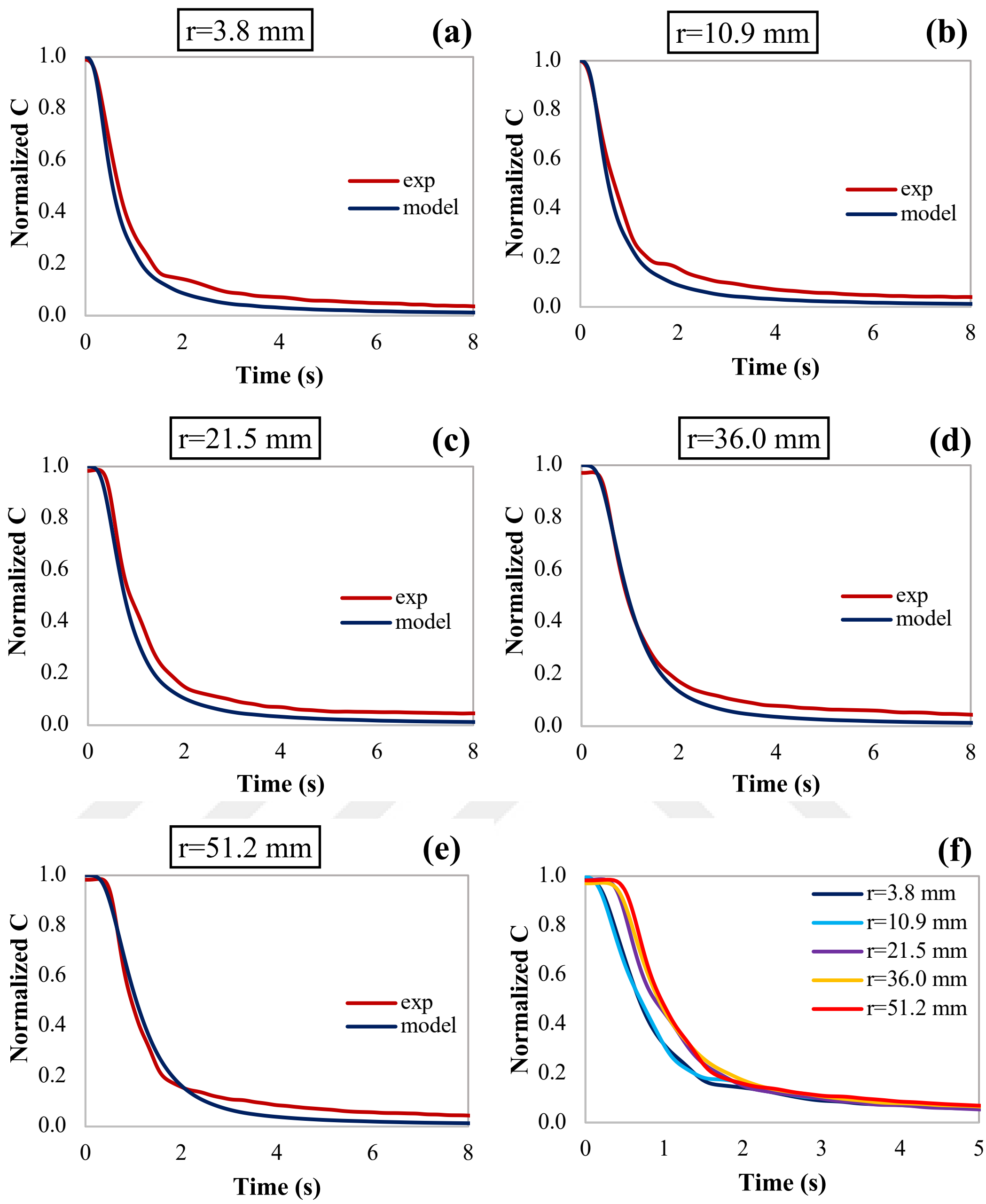

Figure 3.15 Comparison of experimental and predicted tracer concentration profiles at different radial positions (a) r=3.8 mm (Node 13), (b) r=10.9 mm (Node 14), (c) r=21.5 mm (Node 12), (d) r=36.0 mm (Node 9), (e) r=51.2 mm (Node 5), (f) experimental tracer profiles (ρ_p=2460 kg/m^3, d_p=1 mm, γ=30°, H_b=180 mm, U_0=1.25U_{ms}, D=0.0186 m^2/s)

The quality of the fit between the experimental and predicted results varies due to the assumption of constant dispersion coefficient for all streamtubes. As can be seen from the figures the quality of the fit increases with radial position from the center to the wall. The experimental radial profiles of tracer for all conditions show steeper decline at the points near the spout region as expected. Due to the higher velocities in the spout region, the input-output response time in negative step experiments is relatively shorter.

The dispersion coefficients predicted by the gas mixing model are tabulated in Table 3.3. The predicted dispersion coefficients obtained in the repeatability experiments are also presented. The superficial gas velocities at the inlet of the bed were determined based on the minimum spouting velocity and it was set to 1.25 times of U_{ms} as it was mentioned before. The results show that the dispersion coefficient increases with the increasing gas velocity and decreasing cone angle. Since the stagnant bed height of the 30° spouted bed is higher than the 60° spouted bed, all particles have higher minimum spouting velocities and as the particle density increases, this effect becomes more significant which result in the higher superficial gas velocities at the inlet of the bed. At the end, the increase in the dispersion coefficient with decreasing cone angle can be related with the increasing gas velocity.

For comparison purposes, dispersion coefficients calculated by using the correlation proposed by San Jose et al. (1995) (Eq. 3.1 and Eq. 3.2) for same operating conditions are also presented in Table 3.3. The dispersion coefficients predicted by the correlation of San Jose et al. (1995) underestimate the experimentally determined values in this work for all cases; the difference being more pronounced (almost an order of magnitude of discrepancy) for 30^0 conical angle compared to 60^0.

The correlation gives more satisfactory results for glass beads particles for conical spouted bed having conical angle of 60^0. As the particle density increases, the validity of the correlation decreases. For 30^0 conical spouted bed, close match of the dispersion coefficients could not be determined.

Table 3.4 The dispersion coefficients predicted by the gas mixing model and calculated ones with San Jose et al.'s correlation

	Particle	ρ_p (kg/m^3)	D (m^2/s)	D (m^2/s) San Jose et al. (1995)	% difference between dispersion coefficients
60°	Zirconia (Exp1)	6050	0.0608	0.01912	%68.55
	Zirconia (Exp2)	6050	0.0648		%70.49
	Alumina (Exp1)	3700	0.0469	0.0152	%67.59
	Alumina (Exp2)	3700	0.0465		%67.31
	Glass Beads (Exp1)	2460	0.0175	0.0126	%28.00
	Glass Beads (Exp2)	2460	0.0179		%29.61
30°	Zirconia	6050	0.0935	0.00584	%93.75
	Glass Beads	2460	0.0186	0.00386	%79.25

The dispersion coefficients obtained in this study are compared with the ones reported in the literature for fluidized and spouted beds in Figure 3.16. For this purpose, the figure developed by San Jose and his co-workers (1995) was used. They included the literature values and their experimental results obtained in conical spouted beds. The dispersion coefficients calculated by using the correlation of San Jose et al. (1995) which were in the range of $2.6x10^{-4}$ m^2/s and $6.1x10^{-2}$ m^2/s are also included in the figure. The dispersion coefficients obtained in this study are higher than the corresponding dispersion coefficients of fixed beds, lower than the corresponding dispersion coefficients of fluidized beds and similar with the corresponding dispersion coefficients in cylindrical spouted beds available in the literature.

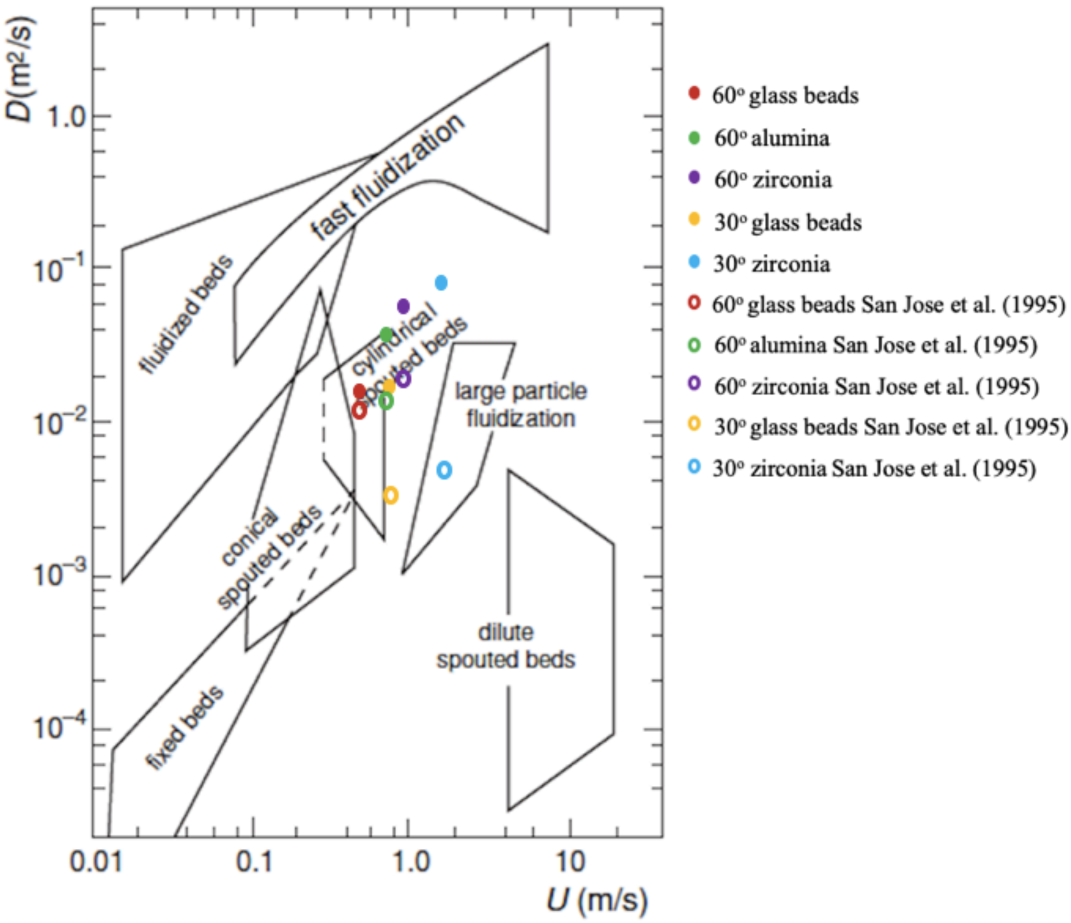

Figure 3.16 Comparison of the dispersion coefficients with literature

Peclet number is a dimensionless number used to estimate the ratio of the advective transport to the diffusive transport which is defined with Eq. 3.3 where L is the characteristic axial length of the reactor and U is the characteristic velocity. Peclet number can be used to compare the axial mixing characteristics of reactors of different sizes and operating velocities.

In this study, same definition of Peclet number with Wang (2006) was used and radial distributions of the Peclet numbers for systems and operating conditions were calculated in the range of 0.56-7.84 and the results are tabulated in Table 3.4 below.

Table 3.5 Peclet numbers for all experimental conditions

	Particle	ρ_p (kg/m^3)	Peclet Numbers
60°	Zirconia	6050	0.56-2.18
	Alumina	3700	0.59-2.30
	Glass Beads	2460	1.13-4.42
30°	Zirconia	6050	0.65-2.40
	Glass Beads	2460	2.13-7.84

Because, the streamtube length increases as the radial distance increases, Peclet numbers also tend to increase with radial distance. The results show that Peclet numbers have higher values for spouted beds having narrower angle or for lower density particles compared to the higher density particles. This indicates that convection become more significant than dispersion with decreasing particle density and conical angle.

3.6 Conclusion

In this chapter, results of axial gas mixing experiments are presented for conical spouted beds operated with both low- and high-density particles. An axial gas mixing model based on San Jose (1995) was developed and implemented in MATLAB to determine the dispersion coefficients. The results show that the dispersion coefficients for conical spouted beds range between $1.75x10^{-2}$ m^2/s and $9.35x10^{-2}$ m^2/s increasing with increasing superficial gas velocity and decreasing with cone angle. The Peclet numbers calculated in the range of 0.56-7.84 revealed that the convective transport was more dominant than axial dispersion for light particles compared to heavy particles and it was favored by lower conical angle.

CHAPTER 4

CONCLUSIONS & RECOMMENDATIONS

4.1 Conclusion

In this thesis, results of Pitot tube measurements for axial gas velocity and negative step tracer gas experiments for axial gas mixing are presented for conical spouted beds operated with both low- and high-density particles. Experiments were conducted in two small scale (D_c = 150 mm, γ = 30º, 60º) and one large scale (D_c = 250 mm, γ = 66º) conical spouted beds by using three different type of particles which are zirconia (ρ_p = 6050 kg/m^3), zirconia toughened alumina (ρ_p = 3700 kg/m^3) and glass beads (ρ_p = 2460 kg/m^3) as bed materials. Effect of axial position, conical angle, bed size and particle density on the local gas velocity profiles were investigated and the amount of inlet gas passing through the regions were calculated. For detailed understanding of the gas mixing characteristics of the conical spouted beds, a gas mixing model was proposed based on the model of San Jose et al. (1995). The gas velocity results obtained by Pitot tube measurements were used in the gas mixing model. The gas mixing model was implemented in MATLAB and the axial dispersion coefficients and corresponding Peclet numbers were determined for different design and operating conditions. The general conclusions of this thesis based on the experimental and model results can be stated as follows:

- A system that measures the local gas velocities in conical spouted beds accurately was developed. Careful calibration of the Pitot tube for determination of gas velocities in the annulus section was carried out in a separate loosely packed bed set-up, which represents the flow conditions in the annulus section of the spouted bed. Solids hold-up profiles were used to calculate the superficial gas velocities and determine the amount of air flowing through the spout, interface, and annulus.

- For both light and heavy particles, the local gas velocity profiles are significantly affected by the axial distance. As the axial distance increases, the interstitial gas velocity decreases rapidly both in the spout and annulus and then levels off. Furthermore, the amount of inlet gas flowing through the annulus increases with axial distance which indicates cross flow from the spout to the annulus.
- The normalized gas velocity in the spout increases and the amount of inlet gas flow through the annulus decreases with increasing cone angle This result shows that the cross flow between spout and annulus regions becomes harder for spouted beds having wider conical angle. Cone angle does not significantly affect the local gas velocity profiles in annulus region.
- The gas flow through the annulus increases with particle density and bed size. The gas is expected to have higher residence time to flow and diffuse to the annulus for large beds. Since most of the inlet gas flows through the spout and interface regions for the small scale bed, the normalized gas velocities in the spout region were found to be also higher compared to the large-scale unit. Furthermore, the effect of bed size on the normalized velocities measured in the spout region is more pronounced for light particles than heavy particles.
- The experimental measurement of the RTD in transient mixing experiments is a challenging task especially for high density particles due to high operational velocities and short residence times.
- The experimental and RTD curves obtained from axial gas mixing model shows close agreement which shows that axial gas mixing in a conical spouted bed can be modeled by a 1-D transient convection-diffusion equation with the assumptions of plug flow in the spout and constant axial dispersion in the annulus.
- The axial dispersion coefficients were found to be in the range of $1.75x10^{-2}$ m^2/s and $9.35x10^{-2}$ m^2/s in the design and operating conditions of this thesis. The dispersion coefficient increases with the increasing gas velocity.

The dispersion coefficient values in this work are higher than those obtained in previous conical spouted bed studies reported in the literature. Furthermore, they are higher than those in fixed beds, lower than those obtained in fluidized beds and in the same order of magnitude with cylindrical spouted beds.

- Peclet numbers are found in the range of 0.56-7.84 and increases with decreasing particle density and cone angle which shows that convection become more significant than dispersion in annulus region for light particles or spouted beds having narrower angle.

The gas velocity and axial gas mixing results can be utilized in design of conical spouted bed reactors.

4.2 Recommendations

This study investigated the local flow structure and gas mixing characteristics of conical spouted beds and the results were compared with the only available correlations which were not based on high density particle data. Therefore, as expected, significant deviations between experimental and correlation results were observed especially for heavy particles. In this respect, a new gas velocity and axial dispersion coefficient correlation valid for both light and high-density particles can be developed as a future work. In addition, the gas mixing model can further be improved by taking the radial gas convection and dispersion into consideration.

REFERENCES

Ali, N., Al-Juwaya, T., & Al-Dahhan, M. (2016). Demonstrating the non-similarity in local holdups of spouted beds obtained by CT with scale-up methodology based on dimensionless groups. Chemical Engineering Research and Design, 114, 129-141. doi:10.1016/j.cherd.2016.08.010

Aradhya, S., Taofeeq, H., & Al-Dahhan, M. (2017). Evaluation of the dimensionless groups based scale-up of gas–solid spouted beds. International Journal of Multiphase Flow, 94, 209-218. doi:10.1016/j.ijmultiphaseflow.2017.04.006

Becker, H. (1961). An investigation of laws governing the spouting of coarse particles. Chemical Engineering Science, 13(4), 245-262. doi:10.1016/0009-2509(61)80021-3

Bi, H. T., Macchi, A., Chaouki, J., & Legros, R. (1997). Minimum spouting velocity of conical spouted beds. The Canadian Journal of Chemical Engineering, 75(2), 460-465. doi:10.1002/cjce.5450750221

Çangal, P. (2011). Gas mixing in conical spouted beds with heavy particles, Master of Science Thesis, Hacettepe University, Ankara, Turkey.

Celaya, E. A., Aguirrezabala, J. J., & Chatzipantelidis, P. (2014). Implementation of an Adaptive BDF2 Formula and Comparison with the MATLAB Ode15s. Procedia Computer Science, 29, 1014-1026. doi:10.1016/j.procs.2014.05.091

Davis, M. E., & Davis, R. J. (2003). Fundamentals of chemical reaction engineering. McGraw-Hill Higher Education.

Elordi, G., Lopez, G., Aguado, R., Olazar, M., & Bilbao, J. (2007). Catalytic Pyrolysis of High Density Polyethylene on a HZSM-5 Zeolite Catalyst in a Conical Spouted Bed Reactor. International Journal of Chemical Reactor Engineering, 5(1). doi:10.2202/1542-6580.1567

Epstein, N., & Grace, J. R. (2011). Spouted and spout-fluid beds: Fundamentals and applications. Cambridge: Cambridge University Press.

Fogler, H. S. (2003). Elements of chemical reaction engineering. Boston: Pearson.

Gear, C. (1971). Numerical initial value problems in ordinary differential equations. Englewood Cliffs, NJ: Prentice-Hall.

Hastie, T. J., & Tibshirani, R. J. (1999). Generalized additive models. Boca Raton, FL: Chapman & Hall/CRC.

Huilin, L., Yongli, S., Yang, L., Yurong, H., & Bouillard, J. (2001). Numerical Simulations of Hydrodynamic Behavior in Spouted Beds. Chemical Engineering Research and Design, 79(5), 593-599. doi:10.1205/02638760152424370

José, M. J., Olazar, M., Alvarez, S., & Bilbao, J. (1998). Local Bed Voidage in Conical Spouted Beds. Industrial & Engineering Chemistry Research, 37(6), 2553-2558. doi:10.1021/ie9707681

José, M. J., Olazar, M., Alvarez, S., Morales, A., & Bilbao, J. (2005). Local porosity in conical spouted beds consisting of solids of varying density. Chemical Engineering Science, 60(7), 2017-2025. doi:10.1016/j.ces.2004.12.004

José, M. S., Olazar, M., Peñas, F., Arandes, J., & Bilbao, J. (1995). Correlation for calculation of the gas dispersion coefficient in conical spouted beds. Chemical Engineering Science, 50(13), 2161-2172. doi:10.1016/0009-2509(95)00079-k

Kulah, G., Sari, S., & Koksal, M. (2016). Particle Velocity, Solids Hold-Up, and Solids Flux Distributions in Conical Spouted Beds Operating with Heavy Particles. Industrial & Engineering Chemistry Research, 55(11), 3131-3138. doi:10.1021/acs.iecr.5b04496

Kunii, D., & Levenspiel, O. (1991). Fluidization Engineering. Boston.

Levenspiel, O. (1979). The chemical reactor minibook. Corvallis (OR): OSU Book Stores.

Lim, C. J., & Mathur, K. B. (1974). Residence time distribution of gas in spouted beds. The Canadian Journal of Chemical Engineering, 52(2), 150-155. doi:10.1002/cjce.5450520203

Lim, C. J., & Mathur, K. B. (1976). A flow model for gas movement in spouted beds. AIChE Journal, 22(4), 674-680. doi:10.1002/aic.690220407

Mamuro, T., & Hattori, H. (1968). Flow Pattern Of Fluid In Spouted Beds. Journal of Chemical Engineering of Japan, 1(1), 1-5. doi:10.1252/jcej.1.1

Mathur, K. B., & Epstein, N. (1974). Spouted beds. New York: Academic Press.

Mostoufi, N., Kulah, G., & Koksal, M. (2015). Flow structure characterization in conical spouted beds using pressure fluctuation signals. Powder Technology, 269, 392-400. doi:10.1016/j.powtec.2014.09.028

Olazar, M., Jose, M. J., Aguayo, A. T., Arandes, J. M., & Bilbao, J. (1992). Stable operation conditions for gas-solid contact regimes in conical spouted beds.

Industrial & Engineering Chemistry Research, 31(7), 1784-1792. doi:10.1021/ie00007a025

Olazar, M., José, M. J., Izquierdo, M. A., Salazar, A. O., & Bilbao, J. (2001). Effect of operating conditions on solid velocity in the spout, annulus and fountain of spouted beds. Chemical Engineering Science, 56(11), 3585-3594. doi:10.1016/s0009-2509(01)00022-7

Olazar, M., José, M. S., Peñas, F., Aguayo, A., Arandes, J., & Bilbao, J. (1995). A simplified model for gas flow in conical spouted beds. The Chemical Engineering Journal and the Biochemical Engineering Journal, 56(2), 19-26. doi:10.1016/0923-0467(94)02847-4

Rojas, I. D. (2010). Preliminary Results for the Investigation of Hydrodynamic Scaling Relationships in Shallow Spouted Beds. Separation Science and Technology, 45(12-13), 1928-1934. doi:10.1080/01496395.2010.494711

Sari, S., Kulah, G., & Koksal, M. (2012). Characterization of gas–solid flow in conical spouted beds operating with heavy particles. Experimental Thermal and Fluid Science, 40, 132-139. doi:10.1016/j.expthermflusci.2012.02.008

Stocker, R. K., Eng, J. H., Svrcek, W. Y., & Behie, L. A. (1989). Ultrapyrolysis of propane in a spouted-bed reactor with a draft tube. AIChE Journal, 35(10), 1617-1624. doi:10.1002/aic.690351005

Thorley, B., Saunby, J. B., Mathur, K. B., & Osberg, G. L. (1959). An analysis of air and solid flow in a spouted wheat bed. The Canadian Journal of Chemical Engineering, 37(5), 184-192. doi:10.1002/cjce.5450370503

Velzen, D. V., Flamm, H. J., & Langenkamp, H. (1974). Gas flow patterns in spouted beds. The Canadian Journal of Chemical Engineering, 52(2), 145-149. doi:10.1002/cjce.5450520202

Wang, Z. (2006). Experimental Studies and CFD Simulations of Conical Spouted Bed Hydrodynamics, Ph. D. Thesis, University of British Columbia, Vancouver, Canada.

Wang, Z., Bi, H., & Lim, C. (2006). Numerical simulations of hydrodynamic behaviors in conical spouted beds. China Particuology, 4(3-4), 194-203. doi:10.1016/s1672-2515(07)60261-9

Yeniçeri, A. (2019). Characterization of local flow behavior in conical spouted beds, Master of Science Thesis, Department of Chemical Engineering, Middle East Technical University, Ankara, Turkey.

Zhou, J. (2008). Characterizing and modeling the hydrodynamics of shallow spouted beds, Ph. D. Thesis, University of Tennessee, Knoxville.

APPENDICES

A. LabVIEW code for pressure measurement

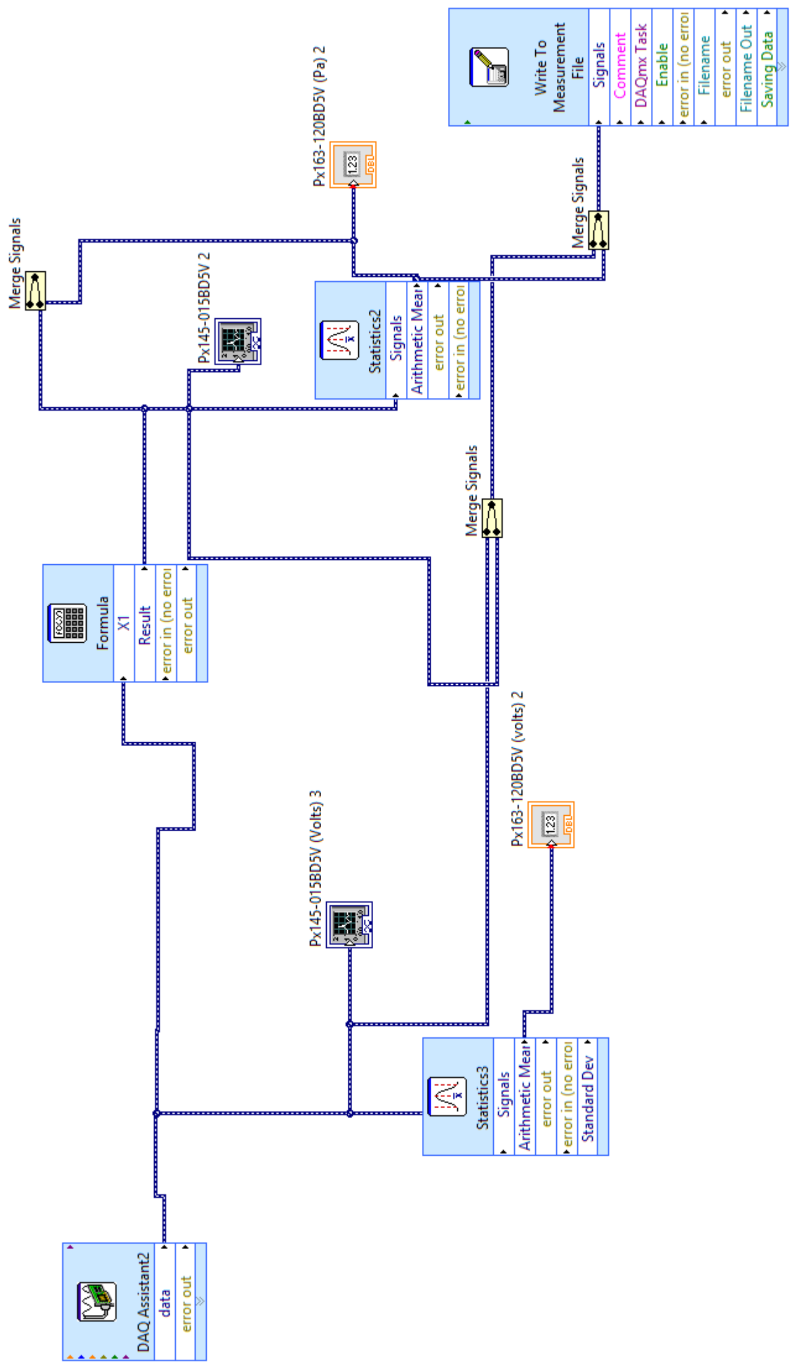

Figure A.1 LabVIEW code for pressure measurement

B. Determination of the voidage profile of conical spouted beds

The Pitot tube measures the interstitial gas velocities. To calculate the amount of air flowing through the system, the superficial gas velocities must be known which is depending on the voidage of the bed as shown in Eq. 2.3. The solids hold-up profiles of the systems were determined by utilizing the empirical correlation developed in our group (Yeniçeri, 2019) given below.

$$\varepsilon_s(0) = 0.043\,\left(\frac{D_b}{D_i}\right)^{0.169}\left(\frac{H_b}{D_o}\right)^{0.435}\left(\frac{U_0}{U_{ms}}\right)^{0.890}\left(\frac{z}{H_b}\right)^{0.816}\gamma^{-0.646} \quad \text{(B.1)}$$

$$\varepsilon(w) = \varepsilon_0\,\left(1+\frac{H_b - z}{H_b}\right)^{0.5} \quad \text{(B.2)}$$

$$\varepsilon = \frac{\varepsilon(0)-\varepsilon(w)}{1+\exp\left((r-r_s)/27.81 r_s^{2.41}\right)} + \varepsilon(w) \quad \text{(B.3)}$$

C. LabVIEW code for concentration measurements

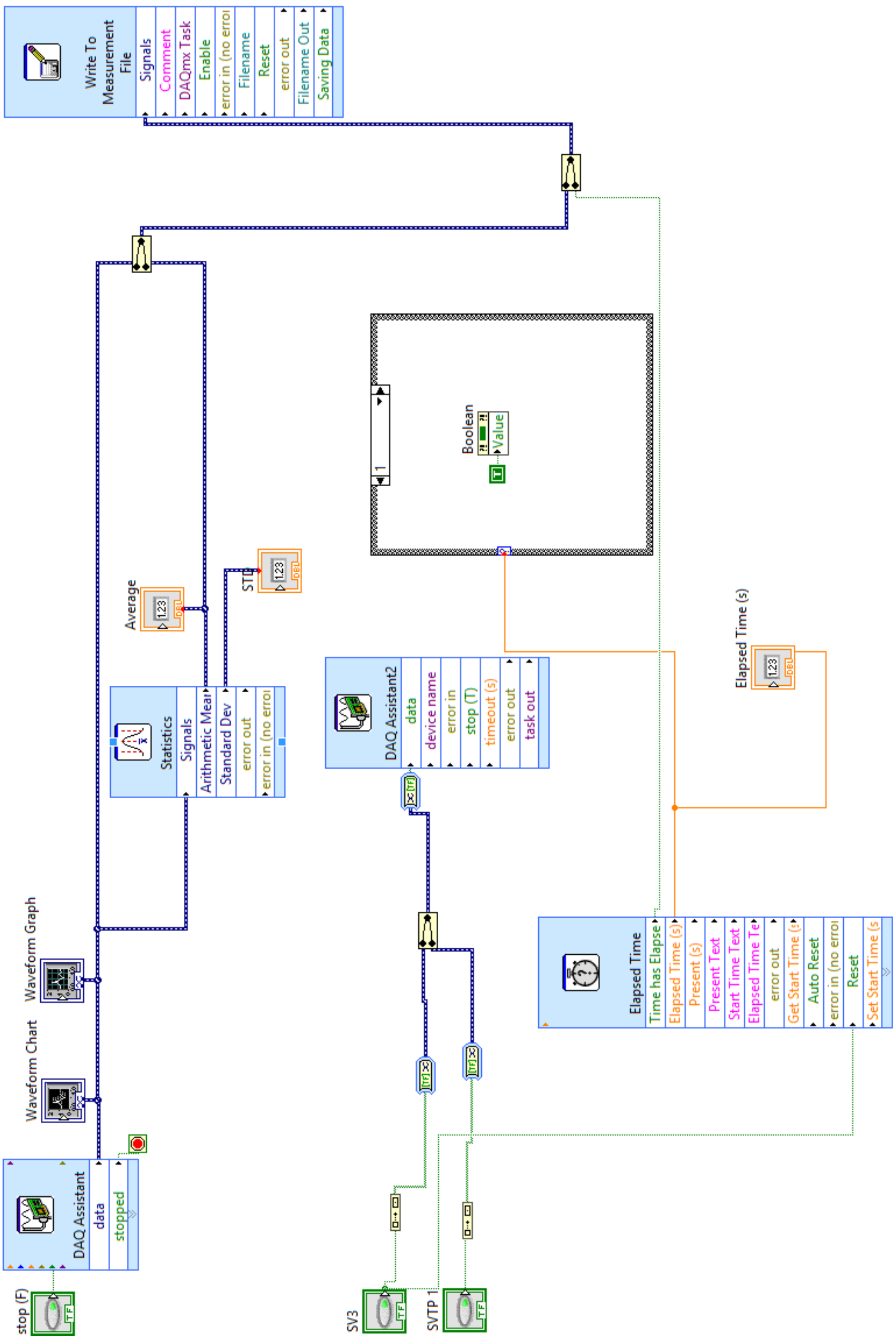

Figure C.1 LabVIEW code for concentration measurements

D. Dimensions of the systems

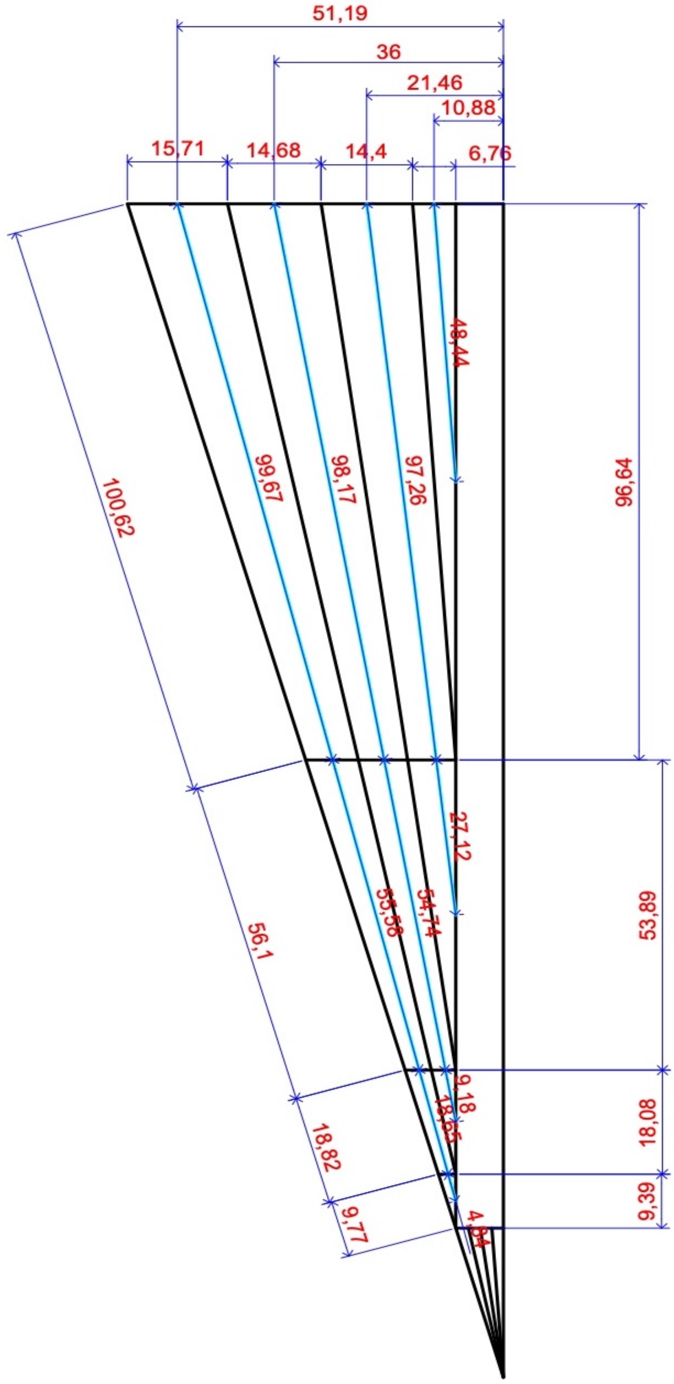

Figure D.1 30° small scale bed dimensions

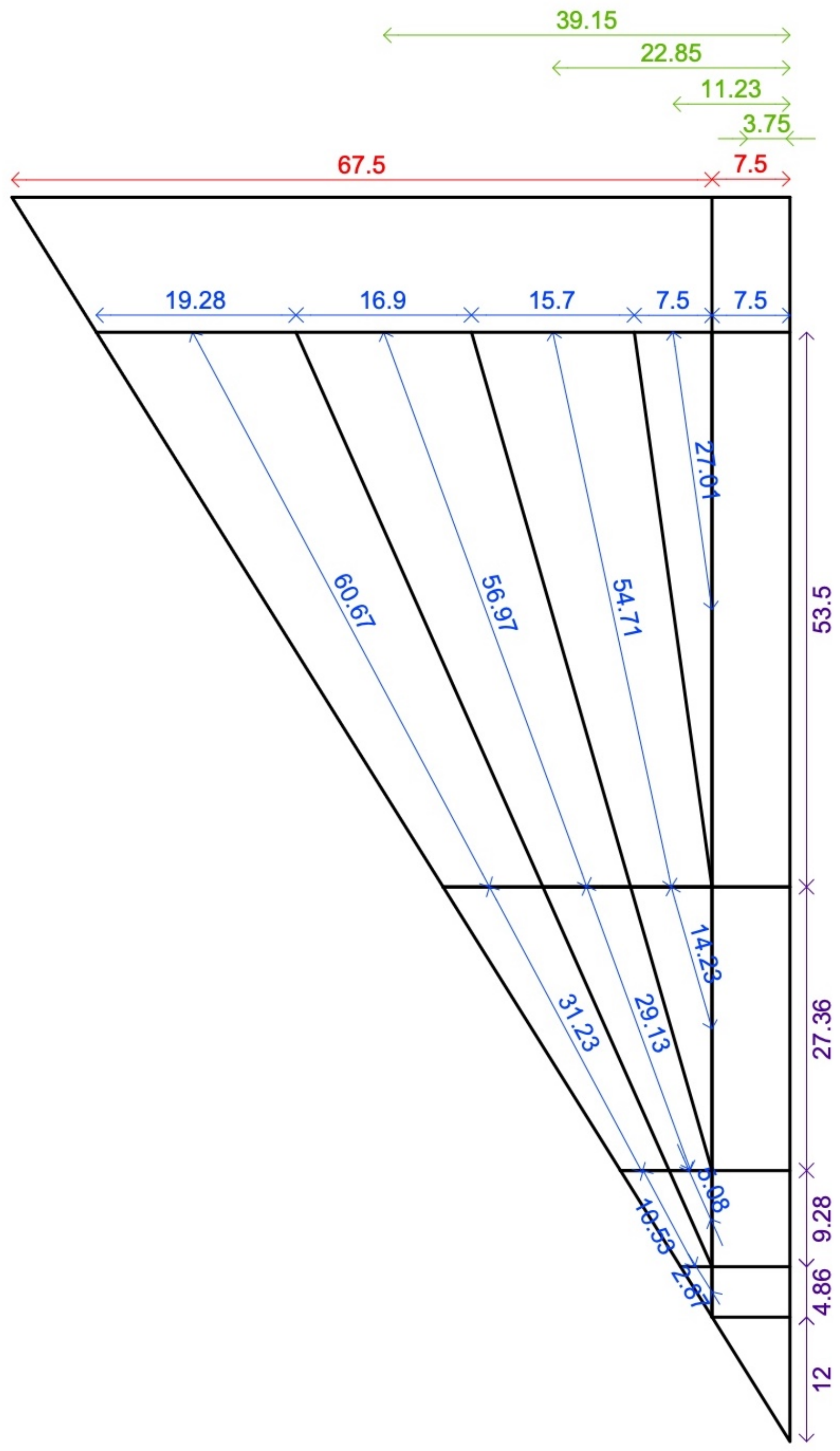

Figure D.2 60° small scale bed dimensions

E. Sample Calculation: 60º small scale conical spouted bed operating with zirconia particles

E1. Determination of the time zero for negative step function

The experiments comprise positive step function, steady state and negative step function. The scope of this study is to investigate the gas mixing behavior of the conical spouted beds by the negative step tracer experiments. Therefore, the time that the valve of the tracer gas closed is accepted time zero both for inlet and the exit of the streamtubes. A magnified region of the negative step function is shown for all nodes at the exit of streamtubes in Figure E.1.

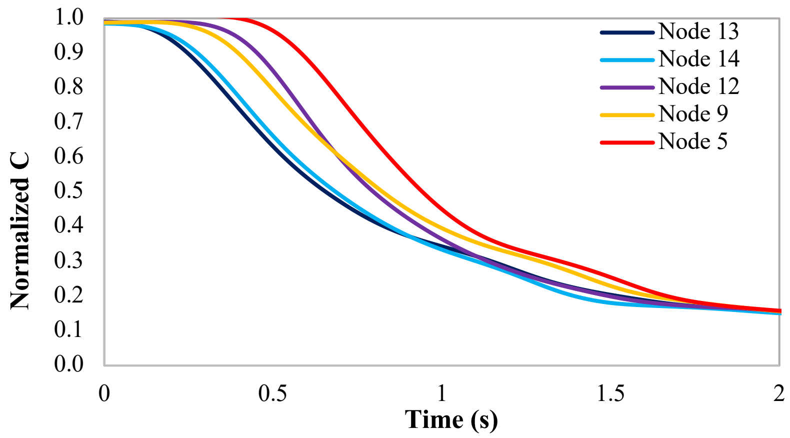

Figure E.1 Experimental data of exit of the streamtubes (ρ_p=6050 kg/m^3, d_p=1 mm, γ=60°, H_b=100 mm, U_0=1.25U_{ms})

E2. Gas velocity in the spout and the annulus

The model requires the knowledge of the local gas velocity both in spout and annulus regions. For annulus region, the gas velocity is almost constant, therefore an average value was calculated. On the other hand, to define the gas velocity depending on position in spout, the results obtained for spout region in Chapter 2 were fitted exponential equations shown in Figure E.2.

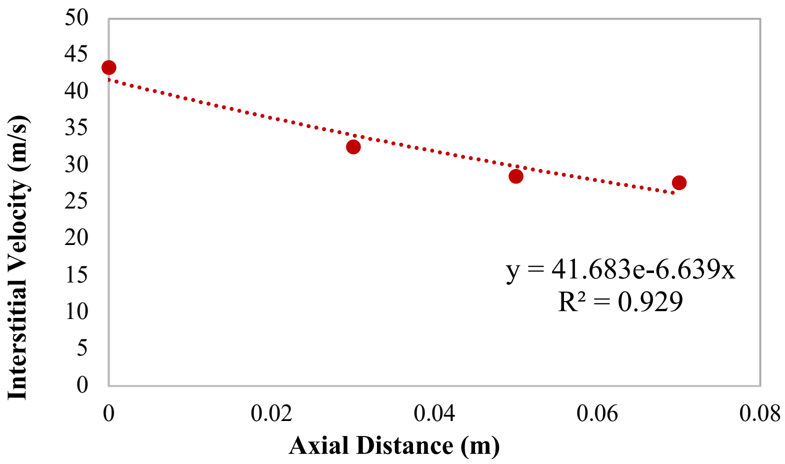

Figure E.2 Interstitial velocity change on axial position in spout (ρ_p=6050 kg/m^3, d_p=1 mm, γ=60°, H_b=100 mm, U_0=1.25U_{ms})

E3. MATLAB Code for tracer concentration distribution in spout

```
function fv=ZRspout(t,C)
global C0

dz=[0.00486 0.00928 0.02736 0.0535] ; %m axial distance

Us=[41.37 39.42 34.81 26.44]; %m/s local gas velocity in spout

fv=zeros(4,1); %number of nodes

    for i=1
        fv(i)=-Us(i)*((C(i)-C0)/dz(i));
    end

    for i=2:4
        fv(i)=-Us(i)*(C(i)-C(i-1))/dz(i);
    end
end


function ZRspoutdistribution
global C0 Cs

IN=xlsread('C:\Users\neslin\Desktop\model\60 deg ZR\60 deg ZR Hb100
1.25 Ums.xlsx','all data negative step','AL3:AL1003');
```

```
k=1;
for j=0:0.01:10.01
    t(k)=j;
    k=k+1;              %definition of time step
end

ic=ones(4,1);           %initial condition

i=1;
m=1;
l=1;

while l<=1001
 C0=IN(i);

[time C]=ode15s(@ZRspout,[t(m):0.005:t(m+1)],ic);

ic=C(end,:);

C(3,:)=[];
time(3,:)=[];
C(2,:)=[];
time(2,:)=[];
Cs(l,:)=[time C];

i=i+1;
m=m+1;
l=l+1;

end

xlswrite('C:\Users\neslin\Desktop\model\60 deg ZR\60 deg ZR Hb100
1.25 Ums.xlsx',Cs,'spout')

end
```

E4. MATLAB Code for tracer concentration distribution in annulus

```
function fv=ZRannulus(t,C)

global D C1 C6 C10 C13 A

dro=[0.00287 0.01053 0.03123 0.06067 0.00508 0.02913 0.05697
0.01423 0.05471 0.02701 ];    %m longitudinal coordinate

Ua=1.25;                      %m/s average gas velocity in annulus

fv=zeros(10,1);               %number of nodes

j=1;
```

```
%streamtube1

        for i=1

            if t==0
               C(i)=1;
            else
               C(i)=(D*C(i+1)+C1*Ua*dro(1))/(Ua*dro(1)+D);
            End

            A(j,1)=C(1);
        end


        for i=2
            fv(i)=(D*(C(i+1)-2*C(i)+C(i-1))/(dro(2)*dro(2)))-
Ua*((C(i)-C(i-1))/dro(2));
        end

        for i=3
            fv(i)=(D*(C(i+1)-2*C(i)+C(i-1))/(dro(3)*dro(3)))-
Ua*((C(i)-C(i-1))/dro(3));
        end


for i=4
            fv(i)=(D*(-C(i)+C(i-1))/(dro(4)*dro(4)))-Ua*((C(i)-C(i-
1))/dro(4));
        end

      %streamtube 2

        for i=5
            if t==0
               C(i)=1;
            else
               C(i)=(D*C(i+1)+C6*Ua*dro(5))/(Ua*dro(5)+D);
            end
            A(j,2)=C(5);
        end

        for i=6
            fv(i)=(D*(C(i+1)-2*C(i)+C(i-1))/(dro(6)*dro(6)))-
Ua*((C(i)-C(i-1))/dro(6));
        end

        for i=7
            fv(i)=(D*(-C(i)+C(i-1))/(dro(7)*dro(7)))-Ua*((C(i)-C(i-
1))/dro(7));
        end
```

```
%streamtube3

        for i=8
            if t==0
               C(i)=1;
            else
               C(i)=(D*C(i+1)+C10*Ua*dro(8))/(Ua*dro(8)+D);
            end
            A(j,3)=C(8);
        end

        for i=9
            fv(i)=(D*(-C(i)+C(i-1))/(dro(9)*dro(9)))-Ua*((C(i)-C(i-
1))/dro(9));
        end

      %streamtube4
        for i=10
            if t==0
               C(i)=1;
            else
               C(i)=(D*C(i)+C13*Ua*dro(10))/(Ua*dro(10)+D);
            end
            A(j,4)=C(10);
        end

end
function ZRannulusdistribution

global D C1 C6 C10 C13 A

Cs=xlsread('C:\Users\neslin\Desktop\model\60 deg ZR\60 deg ZR Hb100
1.25 Ums.xlsx','spout');

Cexp=xlsread('C:\Users\neslin\Desktop\model\60 deg ZR\60 deg ZR
Hb100 1.25 Ums.xlsx','exp exit','B1:F1001');

Cs1=Cs(:,2);
Cs6=Cs(:,3);
Cs10=Cs(:,4);
Cs13=Cs(:,5);

D=0;
x=1;

while x<=1000

ic=ones(10,1);
k=1;
for j=0:0.01:10.01
    t(k)=j;
    k=k+1;
end
```

```
i=1;
m=1;
l=1;

while l<=1001

C1=Cs1(i);
C6=Cs6(i);
C10=Cs10(i);
C13=Cs13(i);

[time C]=ode15s(@ZRannulus,[t(m):0.005:t(m+1)],ic);

C(3,1)=A(1,1);
C(3,5)=A(1,2);
C(3,8)=A(1,3);
C(3,10)=A(1,4);

ic=C(end,:);
C(3,:)=[];
time(3,:)=[];
C(2,:)=[];
time(2,:)=[];
Ca(l,:)=[time C];

i=i+1;
m=m+1;
l=l+1;

end

CONC(:,1)=Ca(:,1);       %time
CONC(:,2)=Cs1;           %Node 1
CONC(:,3)=Ca(:,2);       %Node 2
CONC(:,4)=Ca(:,3);       %Node 3
CONC(:,5)=Ca(:,4);       %Node 4
CONC(:,6)=Ca(:,5);       %Node 5
CONC(:,7)=Cs6;           %Node 6
CONC(:,8)=Ca(:,6);       %Node 7
CONC(:,9)=Ca(:,7);       %Node 8
CONC(:,10)=Ca(:,8);      %Node 9
CONC(:,11)=Cs10;         %Node 10
CONC(:,12)=Ca(:,9);      %Node 11
CONC(:,13)=Ca(:,10);     %Node 12
CONC(:,14)=Cs13;         %Node 13
CONC(:,15)=Ca(:,11);     %Node 14

Ccal=[CONC(:,14) CONC(:,15) CONC(:,13) CONC(:,10) CONC(:,6)];
%outlet of the streamtubes (node 13-14-12-9-5)
```

```
%step by step SSE calculation

SSE=(Cexp-Ccal);
SSE=SSE.^2;
SSE=sum(SSE,'all');

RESULT(x,:)=[D SSE];

D=D+0.0001;
x=x+1;

end


xlswrite('C:\Users\nesli\Desktop\model\60 deg ZR\60 deg ZR Hb100
1.25 Ums.xlsx',RESULT,'D-SSE')

end
```

The dispersion coefficients and the related SSE were calculated. The dispersion coefficient which gives the minimum SSE was determined and tracer concentration distribution was calculated for whole bed by using this dispersion coefficient.